4-26-2018

Parameters Influencing Electromagnetically Induced Transparency

Margaret A. Fortman
Lake Forest College, fortmanma@lakeforest.edu

Parameters Influencing Electromagnetically Induced Transparency

Abstract
This thesis investigates the parameters of achieving electromagnetically induced transparency, or EIT. The technique of EIT manipulates the properties of atoms to partially cancel the usual absorption of laser light. In this experiment, the effect was observed using the D1 line of rubidium vapor and a Λ -configuration between the degenerate magnetic sublevels of the $5S_{1/2}(F=1)$ and $5P_{1/2}(F=1)$ hyperfine states. Among the parameters investigated were the linear and circular polarization of the light used to drive the transitions, the size of the laser beam used, the effects of the temperature of the rubidium interaction cell on EIT, the density of the rubidium atoms in the interaction cell, and the effects of changing the power of the fields used to drive the transitions. Careful measurements of these parameters were made.

Document Type
Thesis

Distinguished Thesis
Yes

Degree Name
Bachelor of Arts (BA)

Department or Program
Physics

First Advisor
Michael M. Kash

Second Advisor
Nathan Mueggenburg

Third Advisor
Enrique Treviño

Subject Categories
Physics

LAKE FOREST COLLEGE

Senior Thesis

Parameters Influencing Electromagnetically Induced Transparency

by

Margaret A. Fortman

April 26, 2018

The report of the investigation undertaken as a
Senior Thesis, to carry two courses of credit in
the Department of Physics

_____	_____
Michael T. Orr	Michael M. Kash, Chairperson
Krebs Provost and Dean of the Faculty	
	_____
	Nathan Mueggenburg
	_____
	Enrique Treviño

ABSTRACT

This thesis investigates the parameters of achieving electromagnetically induced transparency, or EIT. The technique of EIT manipulates the properties of atoms to partially cancel the usual absorption of laser light. In this experiment, the effect was observed using the D1 line of rubidium vapor and a Λ-configuration between the degenerate magnetic sublevels of the $5S_{1/2}(F=1)$ and $5P_{1/2}(F=1)$ hyperfine states. Among the parameters investigated were the linear and circular polarization of the light used to drive the transitions, the size of the laser beam used, the effects of the temperature of the rubidium interaction cell on EIT, the density of the rubidium atoms in the interaction cell, and the effects of changing the power of the fields used to drive the transitions. Careful measurements of these parameters were made.

ACKNOWLEDGMENTS

I owe almost everything I know about physics (and more) to Dr. Kash, Dr. Mueggenburg, and Dr. Schappe. They are each incredible professors, mentors, and people. I owe Dr. Schappe for making me want to become a physics major freshman year, Dr. Kash for making it impossible for me not to sophomore year, and Dr. Mueggenburg for making me really glad I did junior year. To thank Dr. Kash for everything he has done to go above and beyond his duty of being an advisor would take almost as long as this thesis. Instead, I will just say that the passion he has for teaching and the care he shows for his students is more than I thought possible and is undoubtedly one of the best things at Lake Forest College. I certainly cannot express in words how much I am going to miss his lectures, jokes, dinners, and advice.

I am also grateful to all of my fellow physics majors. I'd especially like to thank Robby Mecham and Sean Tilton for going through everything with me this year. The very long nights studying for the GRE, the stress of applying to grad school, and seemingly impossible task of writing our theses were all infinitely more survivable because of them. I would like to thank Robby for being a great friend, lab partner, and a source of competition in the 14 classes we had together. The past four years would not have been nearly as fun without him and his constant humor. I'd also like to thank Sean for being a great friend to share both Dr. Kash's lab and the joys of tutoring with, always having the best puns, and the many rides to get food. I know Robby and Sean will both be extremely successful at ASU and I will miss being there to see it.

I thank Dr. Kash, Dr. Mueggenburg, Dr. Schappe, Robby Mecham, Sean Tilton, and the entire physics department for making me forever grateful I chose Lake Forest College, and I would also like to blame them for making it really, really hard to leave.

TABLE OF CONTENTS

I. INTRODUCTION

Imagine a light beam (with a certain frequency) is shone at a medium that absorbs the light. Now we shine a second light beam with a frequency that will also be absorbed by the medium. Interestingly, the first light beam now gets through the medium as if it were transparent. This is essentially the idea of electromagnetically induced transparency (EIT). We can use laser beams to cause this effect in a medium.

This experiment investigates the parameters that should help us predict how much transmission is expected when the conditions for EIT are met. Since circularly polarized light is crucial for driving the specific transitions in our rubidium atoms, we put much work into improving and characterizing our circular polarization. We also investigated the effects of temperature of the interaction cell, density of atoms in the cell, and changing the power of the fields on our transmission.

In this thesis we will introduce electromagnetic waves and their polarization. Then we will go through the quantum theory of how we drive transitions in atoms to cancel absorption. Next we will detail the apparatus used in this experiment. Lastly, we will see how the concepts above were used in our experiment and present the effects of certain parameters on EIT.

II. THEORY

A. Linear and Circular Polarization

Electromagnetic waves, such as light, are transverse waves made up of an oscillating electric field and magnetic field. The direction of propagation of the wave, the electric field, and the magnetic field are all mutually orthogonal. The Poynting vector, $\vec{S}$, is used to describe the direction of propagation of the wave:[1]

$$\vec{S} = \frac{1}{\mu_o} \vec{E} \times \vec{B} \tag{1}$$

where $\vec{E}$ and $\vec{B}$ are the electric and magnetic fields, respectively. The Poynting vector gives us the energy per unit time per unit area of the wave in the direction of propagation.

By convention, the direction of polarization is defined by the plane in which the electric field component oscillates. Linear polarization occurs when the electric field component of the light wave oscillates in a single plane (as shown in FIG. 1(a)). There are two types of linear polarization used often in this experiment, horizontal polarization and vertical polarization with respect to the laser table. Even more important to our experiment and EIT, however, is getting two circularly polarized beams of light. Circular polarization occurs when the electric field component of the light waves rotate about the direction of propagation (as shown in FIG. 1(b)). Right circularly polarized light is when the electric field appears to rotate in a clockwise direction when looking into the source and left circularly polarized light is when the electric field appears to rotate counterclockwise when looking into the source.

(a) (b)

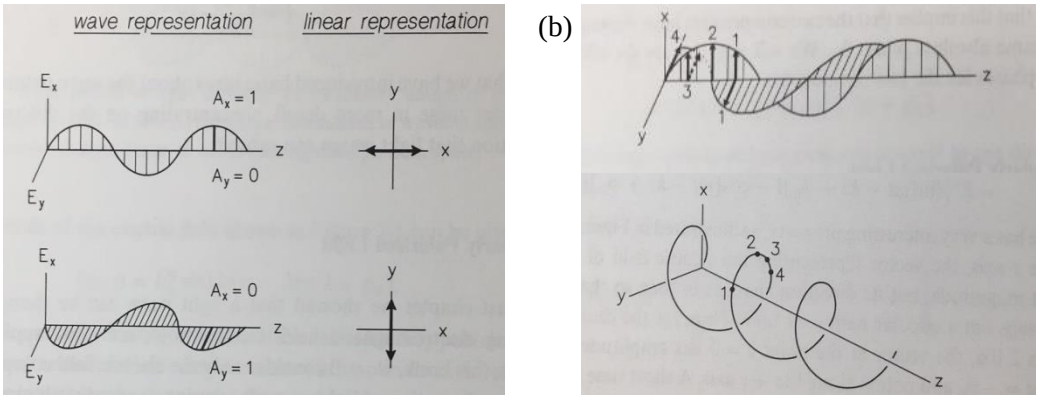

FIG. 1. (a) Linear polarization at different orientations of light propagating in the positive z direction: [top] along the x axis (horizontally polarized) and [bottom] along the y axis (vertically polarized). (b) Right circular polarization: [top] wave representation of orthogonal linear components with equal amplitudes and 90˚ relative phase shift and [bottom] the path at a single instant in time of the electric field vectors.[2]

B. Classical model of EIT

Electromagnetically induced transparency (EIT) is a technique that manipulates the optical properties of atoms by an external field to cancel atomic absorption. It can be used to make an opaque medium transparent through quantum interference[3]. Let's look at a classical model of EIT, a particle mass on a spring, to get a better idea of what this means.

The classical model used to visualize the theory of EIT consists of a simple particle mass on a spring, (FIG. 2). If an electromechanical driver (grey box) applies the resonant frequency of the mass and spring system, which we will call Ω_1, the mass begins to oscillate with an amplitude, A, as shown in FIG. 2(a). Over time, the amplitude, A, will decrease by the damping of the spring. Suppose we now add a second spring to the system, as shown in FIG. 2(b). If we drive the same resonant frequency as we did to the first spring but 180 degrees out of phase, call this Ω_2, the mass will no longer be able to oscillate. The equal and opposite frequencies, Ω_1 and Ω_2, cancel each other out and the mass does not move. There will no longer be any damping on the mass and spring.

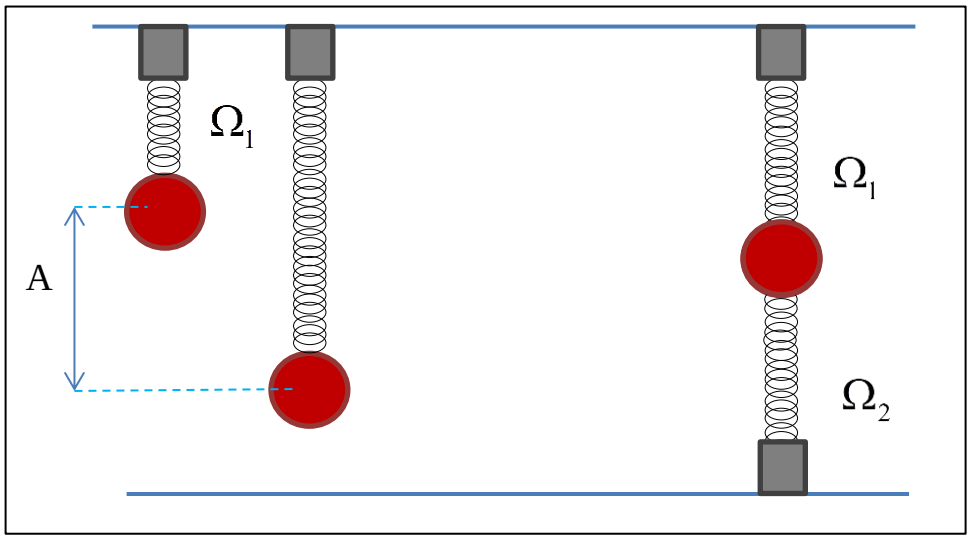

FIG. 2. Classical model of EIT. (a) System 1 consists of a mass and spring with resonant frequency, Ω_1, which is applied by an electromechanical driver (represented by the grey boxes). (b) System 2 consists of a mass and two springs with the same resonant frequencies but 180 degrees out of phase, Ω_1 and Ω_2.

This concept is an excellent analog to the effect of electromagnetically induced transparency. Replace the particle mass and spring in our picture with an electron in an atom and the two drivers with two electromagnetic fields (laser beams) and we have a picture of EIT. We will again start with one field at resonant frequency, this time we will call it Ω_S. The field will excite the electron and cause it to oscillate (as did the mass) with the same frequency as the laser (Ω_S). If we then add a second field to interact with the electron that has the same frequency but opposite polarization, Ω_C, the electron will no longer oscillate. The two fields, we will call them the signal field and control field, cancel each other out and there is no longer any absorption (damping) by the atom.

C. Rubidium Atom

From atomic theory, we know that atoms have quantized energies. Their states are characterized by quantum numbers, each of which has physical significance. For naturally occurring rubidium, there are two isotopes: ^{87}Rb and ^{85}Rb. Since rubidium is an

alkali metal, which means it has one electron in its outer most shell, it can be approximated as a hyrodgenic atom. The outer-most electron occupies the 5S orbital, which has an angular momentum quantum number of $L = 0$. When the atom is excited, it moves up to the next energy level, the 5P orbital ($L = 1$). This excitation, and subsequent decay back down to the 5S orbital, is the transition we will use in this experiment.

1. Fine structure

Quantum theory tells us that the energy levels in an atom are not this simple. Instead, the 5S and 5P orbitals are both shifted and split into sublevels. This is due to the fine structure correction to the energy levels. The fine structure accounts for both the relativistic correction, due to the electron orbiting very fast around the nucleus, and the spin orbit coupling, due to the magnetic field created by the nucleus in the electron's reference frame interacting with the electron's magnetic dipole moment. Therefore, the 5S orbital is shifted down slightly (less energy) due to the relativistic correction, which is the $5^2S_{1/2}$ sublevel. The 5P orbital is both shifted down and split into two distinct levels due to spin-orbit coupling, which become the $5^2P_{1/2}$ and $5^2P_{3/2}$ sublevels. The fine structure is shown in FIG. 3.

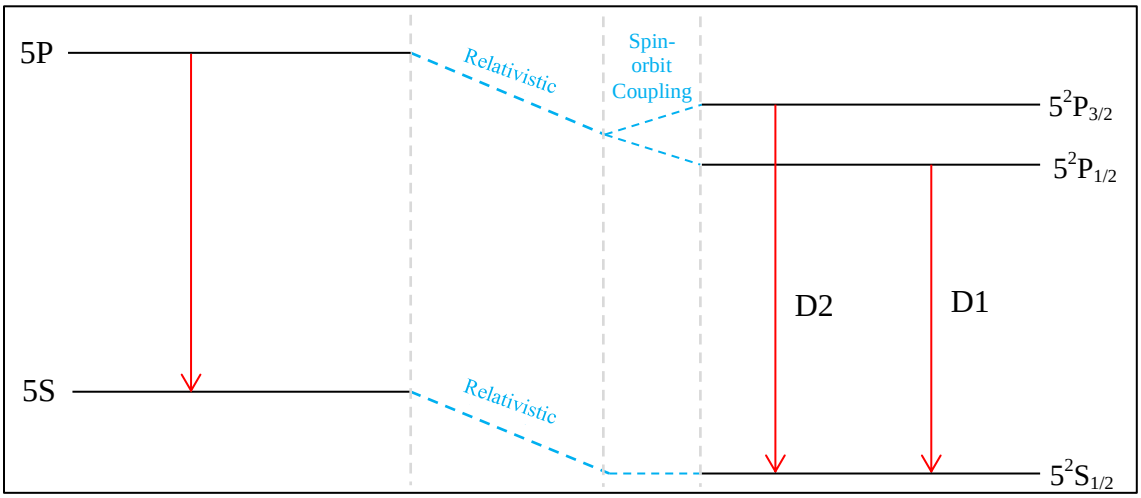

FIG. 3. The fine structure of rubidium. The 5S orbital is shifted by the relativistic correction. The 5P orbital is both shifted by the relativistic correction and split by spin-orbit coupling.

This means that instead of only one possible transition from the 5P to the 5S orbital, there are now two possible transitions. These are labeled the D1 line and the D2 line (D1 being the less energetic of the two). The D1 line corresponds to emitted photons of wavelength $\lambda = 794.979\,\text{nm}$ and the D2 line corresponds to emitted photons of wavelength $\lambda = 780.241\,\text{nm}$.[4] The work done in this experiment solely uses the D1 line, as our laser has a wavelength of 795 nm, therefore we will look more closely at that transition.

2. Hyperfine structure and selection rules

There is another further correction to the energy levels in rubidium, called the hyperfine structure. This is due to the interaction between the intrinsic magnetic dipole moments of the spinning electron and nucleus. This causes the fine structure levels of the D1 line ($5^2P_{1/2}$ and $5^2S_{1/2}$) to be split into two distinct hyperfine levels. These levels are described by their quantum number *F* (total atomic angular momentum). For the D1 line of ^{87}Rb, the quantum numbers are *F*=1 and *F*=2, which can be calculated from the fact that F must be

$$| J - I | \leq F \leq J + I \tag{2}$$

and $\mathrm{I} = \frac{3}{2}$ for ^{87}Rb and $\mathrm{J} = \frac{1}{2}$ for the fine structure levels of the D1 line. These hyperfine levels (*F*=1 and *F*=2) are made up of magnetic sublevels, described by their quantum number, m_F . These can be calculated with the rule

$$-F \leq m_F \leq F\,, \tag{3}$$

which gives us that m_F can be -1, 0, 1 for the *F*=1 level and can be -2, -1, 0, 1, 2 for the *F*=2 level (FIG. 4).

Another very important result from quantum theory are selection rules, which dictate the transitions that may occur between levels in an atom.[5] Specifically, they will tell us the transitions that are allowed to occur between our hyperfine levels and our magnetic sublevels when an atom is excited by circularly polarized light. Quantum selection rules tell us that for a transition between hyperfine levels, *F*,

$$\Delta F = 0, \pm 1. \tag{4}$$

For the D1 line of ^{87}Rb, we will label these transitions as c, d, e, and f, as shown in FIG. 4. The quantum selection rule for transitions between m_F levels tells us that

$$\Delta m_F = \pm 1. \tag{5}$$

We can be even more specific with this rule. If the atom is excited by right circularly polarized light (σ^-),

$$\Delta m_F = -1, \tag{6}$$

and if the atom is excited by left circularly polarized light (σ^+),

$$\Delta m_F = +1. \tag{7}$$

This will be very important in our experiment as it will allow us to essentially choose the transitions we want to occur by applying left and right circularly polarized light to the atoms.

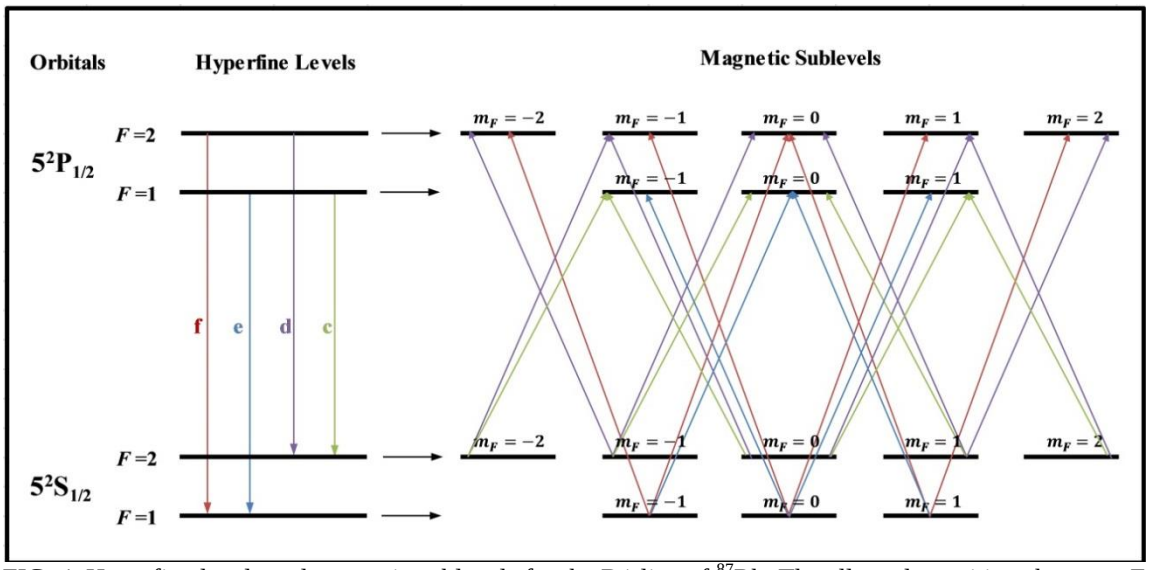

FIG. 4. Hyperfine levels and magnetic sublevels for the D1 line of ^{87}Rb. The allowed transitions between F and m_F levels are shown as well. Adapted from Kevin Spotts' thesis.[6]

C. EIT

In this experiment, we use what is called the Λ-configuration to achieve EIT. The Λ-configuration describes a three-state atomic system, as shown in FIG. 5, in which the possible transitions appear to form the shape of the Greek letter, Λ. We will label the three states $|a\rangle, |b\rangle,$ and $|c\rangle$. In this experiment, the states refer to three magnetic sublevels of ^{87}Rb, two of which are degenerate ($|b\rangle$ and $|c\rangle$). We will use two laser beams to drive the transitions between these states. The two beams give two electromagnetic fields (signal and control field) that cause transitions between these states. We will describe these fields by their Rabi frequency, which is the frequency of the fluctuations in the populations of the two states involved in the transition. The control field, with Rabi frequency Ω_C, couples states $|b\rangle$ and $|a\rangle$, allowing transitions between them. The signal field, with Rabi frequency Ω_S, couples states $|c\rangle$ and $|a\rangle$. As was explained in the classical model, we can apply these frequencies with a laser to attain destructive interference, which will cause the absorption of the atoms to cancel.

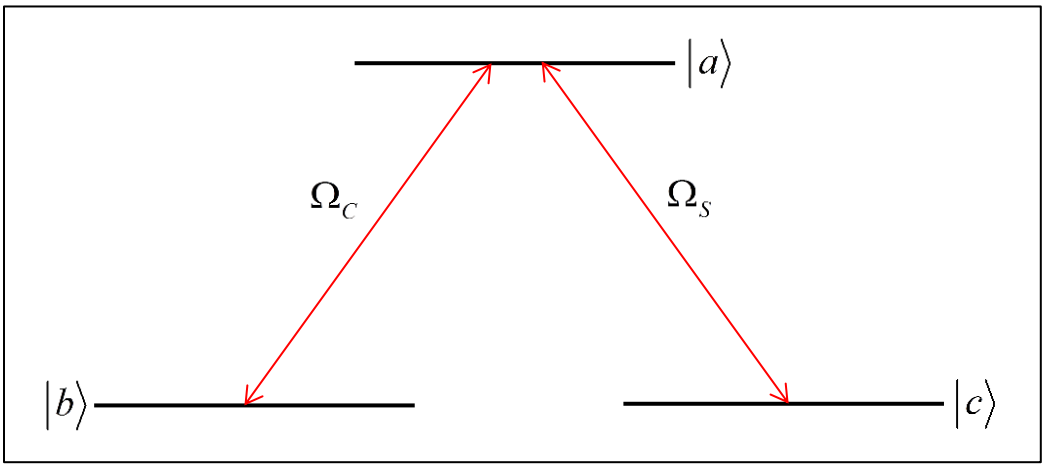

FIG. 5. The Λ - configuration with states $|a\rangle, |b\rangle,$ and $|c\rangle$. The control field, with Rabi frequency Ω_C, couples states $|b\rangle$ and $|a\rangle$ and the signal field, with Rabi frequency Ω_S, couples states $|c\rangle$ and $|a\rangle$.

We define the Rabi frequency for the signal and control fields by,

$$\Omega_C = \frac{-\boldsymbol{\mu}_{ab} \cdot \mathbf{E_C}}{\hbar}, \tag{8}$$

and

$$\Omega_S = \frac{-\boldsymbol{\mu}_{ac} \cdot \mathbf{E}_S}{\hbar}, \tag{9}$$

where $\boldsymbol{\mu}_{ab}$ is the electric dipole moment from $|a\rangle$ to $|b\rangle$, $\mathbf{E_C}$ is the vector electric field amplitude of the control field, $\boldsymbol{\mu}_{ac}$ is the electric dipole moment from $|a\rangle$ to $|c\rangle$, and $\mathbf{E_S}$ is the vector electric field amplitude of the signal field.

Quantum theory allows us to create a new system of 3 states, $|a\rangle, |B\rangle,$ and $|D\rangle$ (FIG. 6), that is a linear combination of the original states, $|a\rangle, |b\rangle,$ and $|c\rangle$. The state $|B\rangle$ is termed the "bright state" and allows transitions up to the $|a\rangle$ state. The state $|D\rangle$ is the "dark state" as it does not allow any transitions up to the $|a\rangle$ state. When an atom is in

state $|a\rangle$ it can decay to state $|B\rangle$ or $|D\rangle$ with equal probability. The atoms that decay to $|D\rangle$ are then trapped since the lasers do not couple $|D\rangle$ to $|a\rangle$. Eventually, all atoms will end up in state $|D\rangle$ and no absorption occurs.

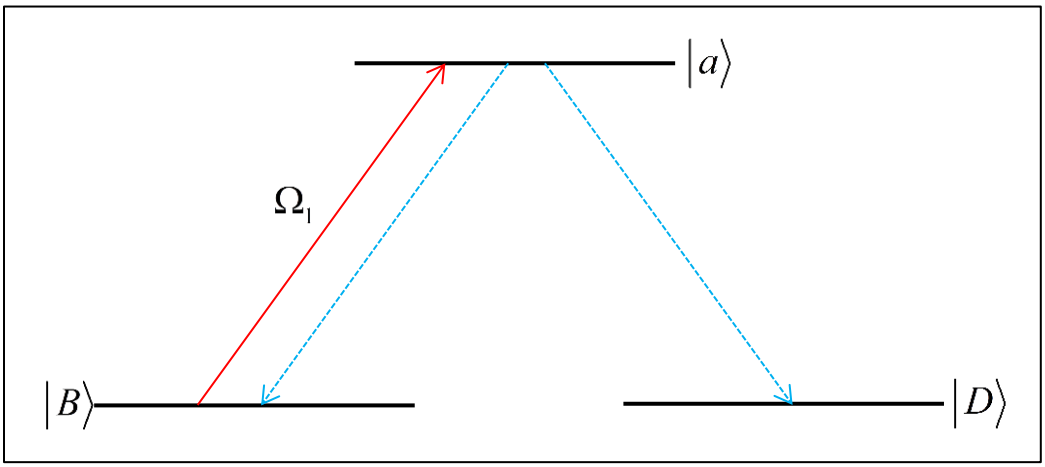

FIG. 6. In the new system the bright state $|B\rangle$ couples to $|a\rangle$, but $|D\rangle$ does not couple to $|a\rangle$. Therefore transitions from $|B\rangle$ to $|a\rangle$ may occur but transitions from $|D\rangle$ to $|a\rangle$ cannot occur. When the atoms are in state $|a\rangle$ they can decay to state $|B\rangle$ or state $|D\rangle$. Eventually all atoms will end up in state $|D\rangle$ and no absorption will occur.

In this experiment, we achieved EIT using the $5^2S_{1/2}$(F=1) to $5^2P_{1/2}$(F=1) transition on the D1 line of ^{87}Rb. The Λ-configuration involves the magnetic sublevels $m_F = -1$ and $m_F = 1$ of the F=1 hyperfine level, which are excited to the $m_F = 0$ magnetic sublevel of the F=1 hyperfine level. A diagram of the Λ-configuration we used is shown in FIG. 7. Transitions were driven from $|F = 1, m_F = -1\rangle$ to $|F = 1, m_F = 0\rangle$ by the control field with left circularly polarized light, σ^+. Transitions were driven from $|F = 1, m_F = 1\rangle$ to $|F = 1, m_F = 0\rangle$ by the signal field with right circularly polarized light, σ^-.

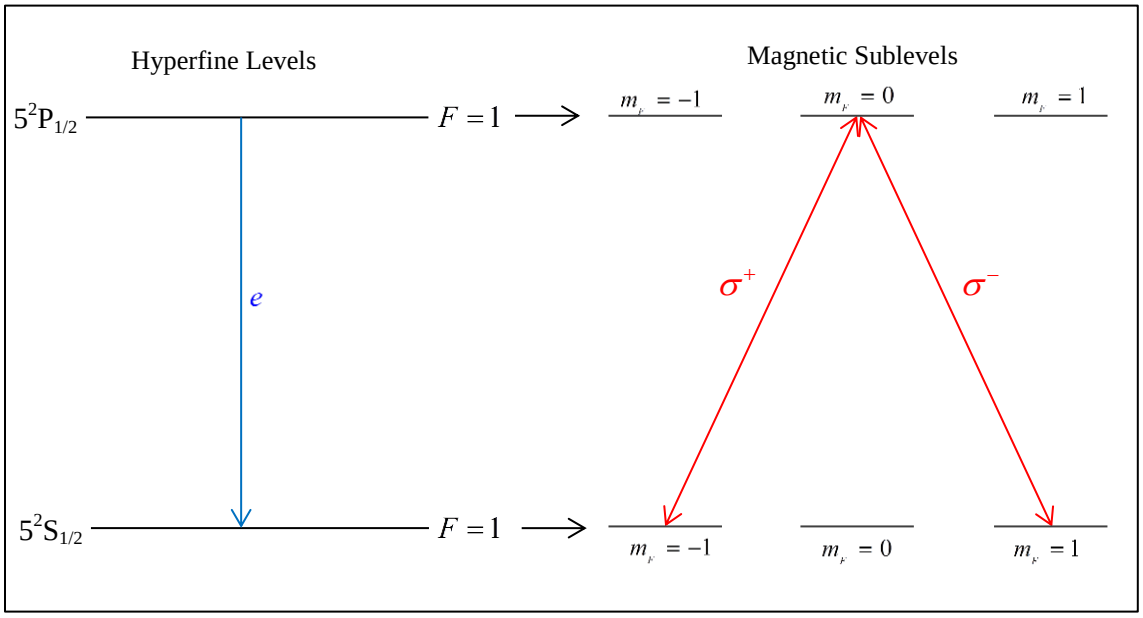

FIG. 7. The Λ - configuration used in this experiment to achieve EIT. Transitions are driven by right circularly polarized light, σ^-, and left circularly polarized light, σ^+.

III. THE APPARATUS

In this section, we will look at exactly how the experiment works through each part of the setup. We will detail the purpose of each instrument. Similar setups have been used in projects before this one, therefore, there are more detailed explanations of parts of the apparatus in the works of Dawson Nodurft (LFC ’10), David Curie (LFC ’13), and Kevin Spotts (LFC ’14). The following (FIG. 8) is an overhead picture of the experimental apparatus.

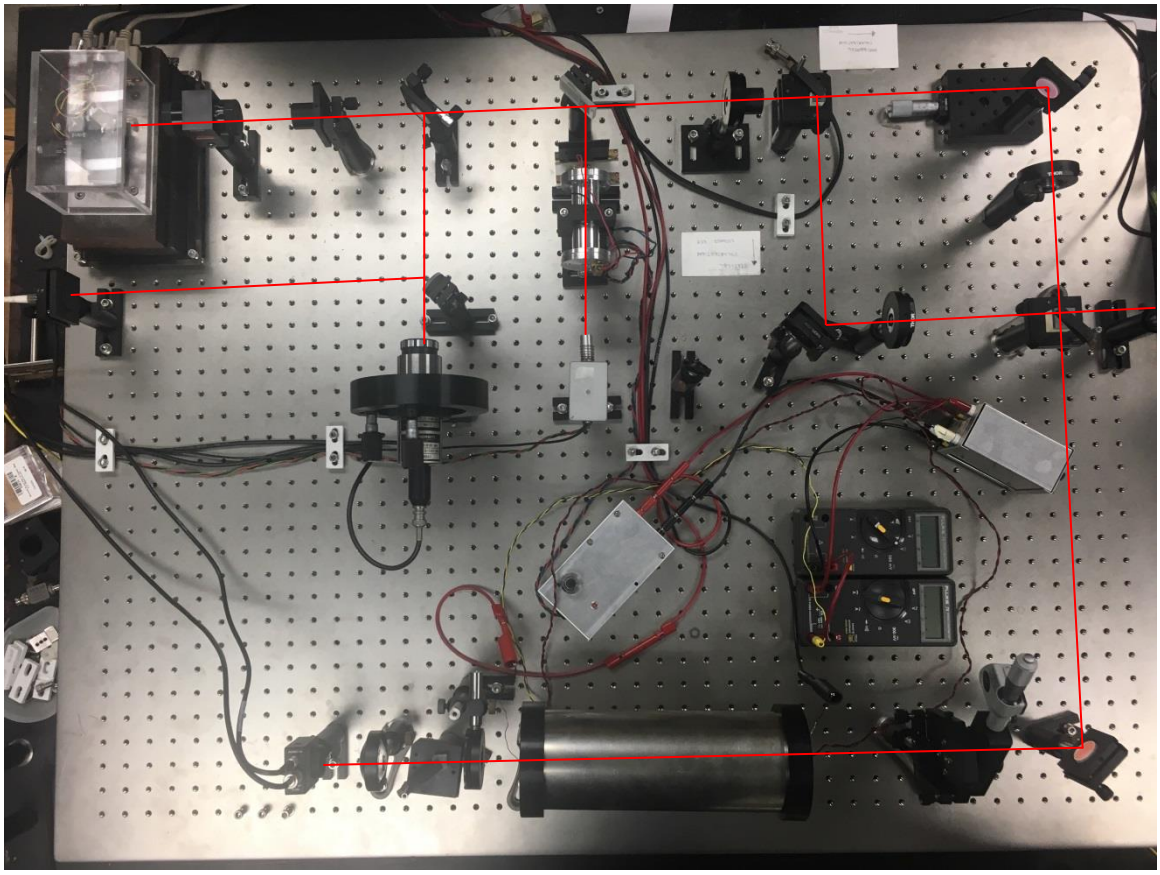

FIG. 8. Overhead picture of the experimental setup.

In attempt to provide a simple and clear representation of the setup, a schematic diagram of the apparatus is shown in FIG. 9, which can be more easily followed.

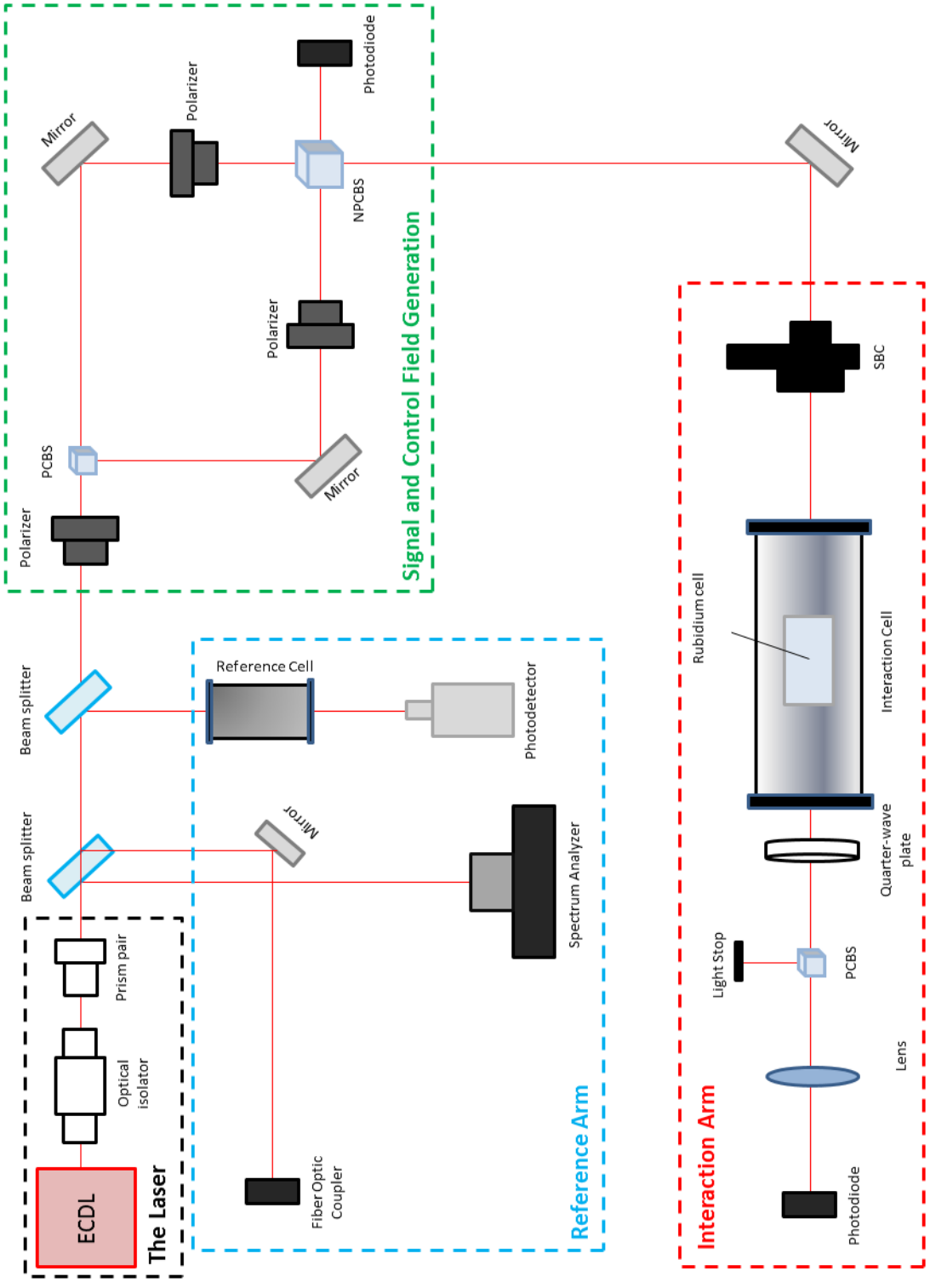

FIG. 9. A schematic overview of the apparatus used in this experiment.

A. Overview of the setup

The setup for this experiment can be divided into four sections: the laser, the reference arm, the signal and control field generation section, and the interaction arm. Each of these has a different role in our overall goal of achieving EIT. The laser section consists of the external cavity diode laser (ECDL) itself, an optical isolator, and a prism pair. The purpose of this section is to produce and modify the laser beam to be used in this experiment. The reference arm consists of a reference cell, photodetector, spectrum analyzer, and fiber optic coupler. This section allows us to monitor the laser beam that will be the input for the rest of the experiment. This section is important for us to be able to properly tune the laser with great accuracy. The signal and control field generation section consists of three linear polarizers, two mirrors, a polarizing cube beam splitter, a non-polarizing cube beam splitter, and a photodiode. As the name suggests, this section generates two different fields. We want these fields to be polarized perpendicular to each other and to have a constant phase difference. The last section the beam encounters is the interaction arm. This section consists of a Soleil-Babinet Compensator (SBC), interaction cell, quarter-wave plate, polarizing cube beam splitter, converging lens, and photodiode. This section has multiple jobs: to create left and right circularly polarized beams that are sent through the interaction cell containing rubidium gas, to convert the light back into its horizontal and vertical components, and then to detect the transmission. The manner in which each of these goals is achieved is outlined in the following sections.

B. The Laser

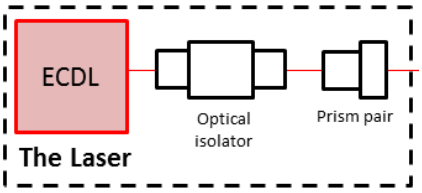

FIG. 10. The Laser section of the apparatus.

This experiment is contingent on having a controlled and steady light source. For this, we rely on an external cavity diode laser, ECDL, which gives us an infrared (795nm) laser beam. The ECDL has been studied by many before us and has been determined to be the best source of light for this experiment. The light coming out of the laser is linearly polarized and has an elliptical cross-section. The first step is to send the beam through an Isowave Model I-80-T4-L optical isolator. The purpose of an optical isolator is to allow light through in a certain direction and block light in the opposite direction, thus preventing back reflections. Therefore, it linearly polarizes our beam (45 degrees from the vertical) and blocks any potentially harmful light from getting back to the laser, which could cause it to become unstable. Next, the beam is sent through a ThorLabs Model PS875-B anamorphic prism pair, which is used to reshape the elliptical beam of the diode laser to a circular beam. The anamorphic prism pair does this by magnifying the elliptical beam in one direction. This gives us the symmetric intensity distribution that is needed.

C. Reference Arm

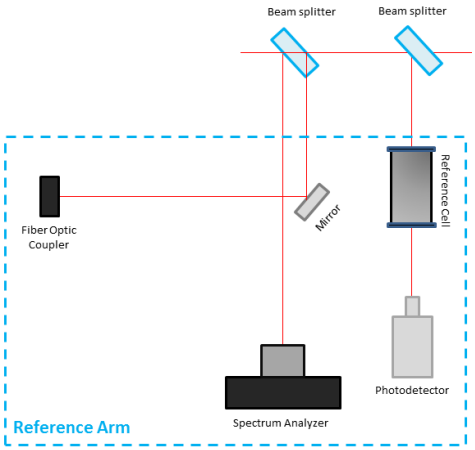

FIG. 11. Reference arm section of the apparatus.

Upon entering the reference arm section of the apparatus, the light encounters a set of beam splitters. The first of the two splits the beam into three different directions: one is directed to a Coherent spectrum analyzer that monitors the laser frequency, one is directed by a mirror to a fiber optic coupler, and the last passes straight through the beam splitter. The light that passes through the first beam splitter encounters the second beam splitter, which directs some light through the reference cell and to a photodetector and the rest passes through. The reference cell contains two isotopes of rubidium, namely ^{85}Rb and ^{87}Rb. Since we are working with ^{87}Rb transitions, this allows us to see its atomic spectrum. The absorption spectrum that we see using an oscilloscope is shown in FIG. 12. This section is vital in our experiment, as it allows us to monitor the laser and tune it to the exact frequency we need to see the transitions of ^{87}Rb. The controls used to tune the laser are detailed later.

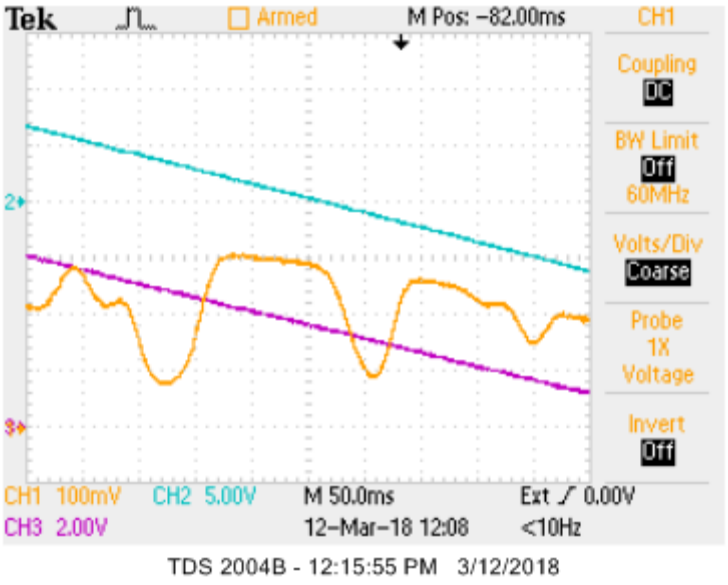

FIG. 12. The yellow line corresponding to Channel 1 monitors the transmission through the reference cell. The dips correspond to transitions in both isotopes of rubidium

D. Signal and Control Field Generation

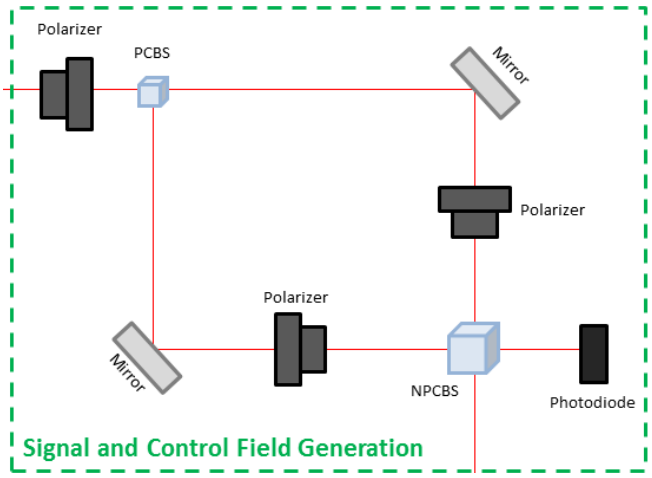

FIG. 13. Signal and Control Field section of the apparatus.

Upon reaching the control field section, the beam is first sent through a ThorLabs Glan-Thompson linear polarizer that ensures the light is linearly polarized at the correct angle. This is important as the beam now reaches a polarizing cube beam splitter (PCBS). The PCBS takes the input beam and produces two output beams that are polarized perpendicular to each other. As shown in FIG. 14, the transmitted beam is horizontally

polarized and the reflected beam is vertically polarized. If the input light into the PCBS is polarized at 45 degrees from the vertical, we get output beams that have equal intensity, as explained subsequently using Malus' Law. This, however, did not correspond to equal intensity beams after the PCBS. Instead, the linear polarizer was adjusted to 36 degrees, which gave approximately equal intensity beams exiting this section.

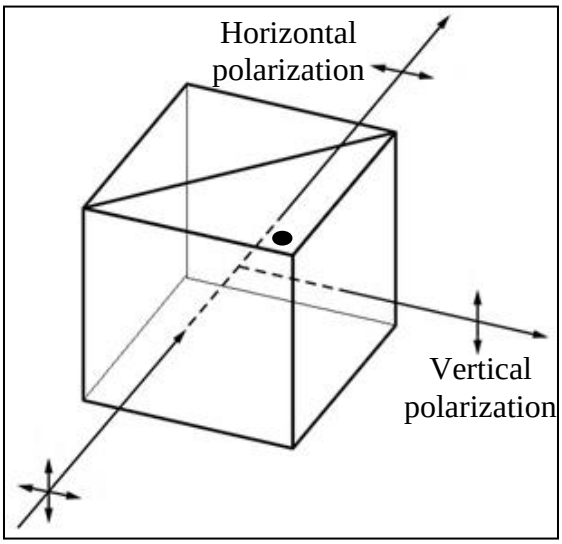

FIG. 14. This diagram shows the transmission and reflection of light through a PCBS. The transmitted beam is horizontally polarized and the reflected beam is vertically polarized.[7]

Now that we have two beams from the PCBS, each is directed by a mirror and through a linear polarizer. These linear polarizers simply assure that the horizontally polarized beam from the PCBS is perfectly horizontally polarized and the vertically polarized beam is perfectly vertically polarized. Then the beams are recombined using a non-polarizing cube beam splitter (NPCBS). The NPCBS performs the opposite task to the PCBS, as it takes the horizontally and vertically polarized beams and recombines them so that they are overlapping. It is important that these overlap well so that the atoms experience both fields equally; therefore much time was put into aligning the beams so that they are on top of each other.

E. Interaction Arm

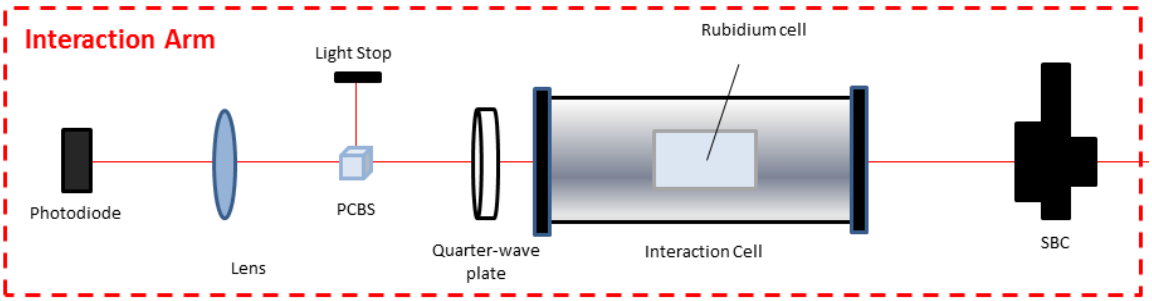

FIG. 15. Interaction Arm section of the apparatus.

The last section that the beam encounters is the interaction arm. The first goal in this section is to achieve circularly polarized light. To do so, we use a ThorLabs Soleil-Babinet Compensator (SBC), the performance of which will be discussed later. The SBC creates left and right circularly polarized light, which is sent into the interaction cell. This is a heated cell containing purely isotopic ^{87}Rb, which is inside a solenoid and surrounded by magnetic shielding. The purpose is to create a controlled magnetic field inside the cell that is not affected by any external magnetic fields. After the light interacts with the rubidium vapor, it exits the cell and is sent through a ThorLabs quarter-wave plate to linearly polarize it once again. Therefore, one beam is now horizontally polarized and the other is vertically polarized. When they reach the PCBS next, the beams are split. The horizontally polarized beam passes straight through and the vertically polarized beam gets reflected.

One interesting thing to note is how blocking the horizontal or vertical beam affects the light transmitted through the PCBS and to the photodiode. If we block the vertical beam in the signal and control field generation section, we still get the horizontal beam transmitted through the PCBS and detected by the photodiode. If we block the horizontal beam, no light gets transmitted through the PCBS, rather it is all reflected.

Therefore, no light is detected by the photodiode. If, however, we rotate the quarter-wave plate before the PCBS 90 degrees, the opposite occurs (blocking the vertical beam results in no light detected by the photodiode). This means that how we now have our quarter-wave plate set up, each component of the light (vertical and horizontal) is circularly polarized (right and left) by the SBC and then converted back to the same component of the light (vertical and horizontal). In other words, the horizontal beam goes through the SBC, is converted to circularly polarized light, and then goes through the quarter-wave plate and becomes horizontally polarized again. The corresponding effect occurs with the vertical beam.

The vertically polarized beam that gets reflected by the PCBS is blocked by a beam stop, and the horizontally polarized light continues through to a converging lens. The lens focuses the beam on a ThorLabs Model PDA10A photodiode, which allows us to monitor the field on an oscilloscope. FIG. 16 shows a scan of the transmission through the interaction cell (green line) as well as the transmission through the reference cell (yellow line).

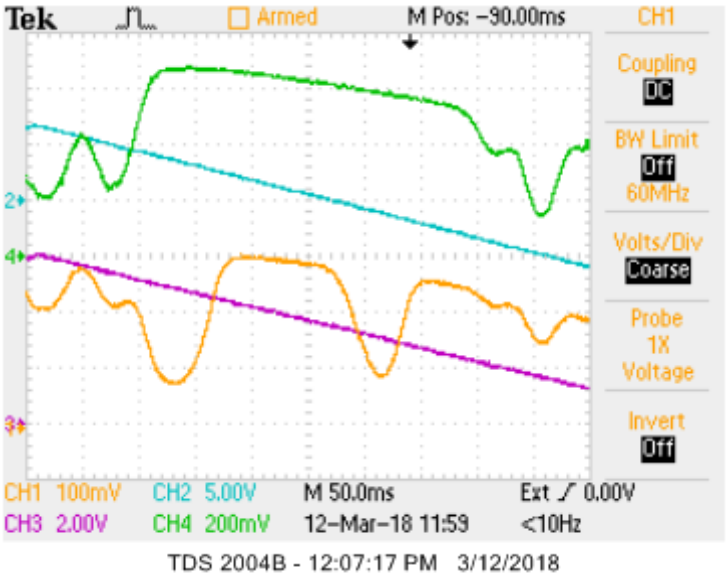

FIG. 16. The yellow line, corresponding to Channel 1, monitors the transmission through the reference cell. The green line, corresponding to Channel 2, monitors the transmission through the interaction cell.

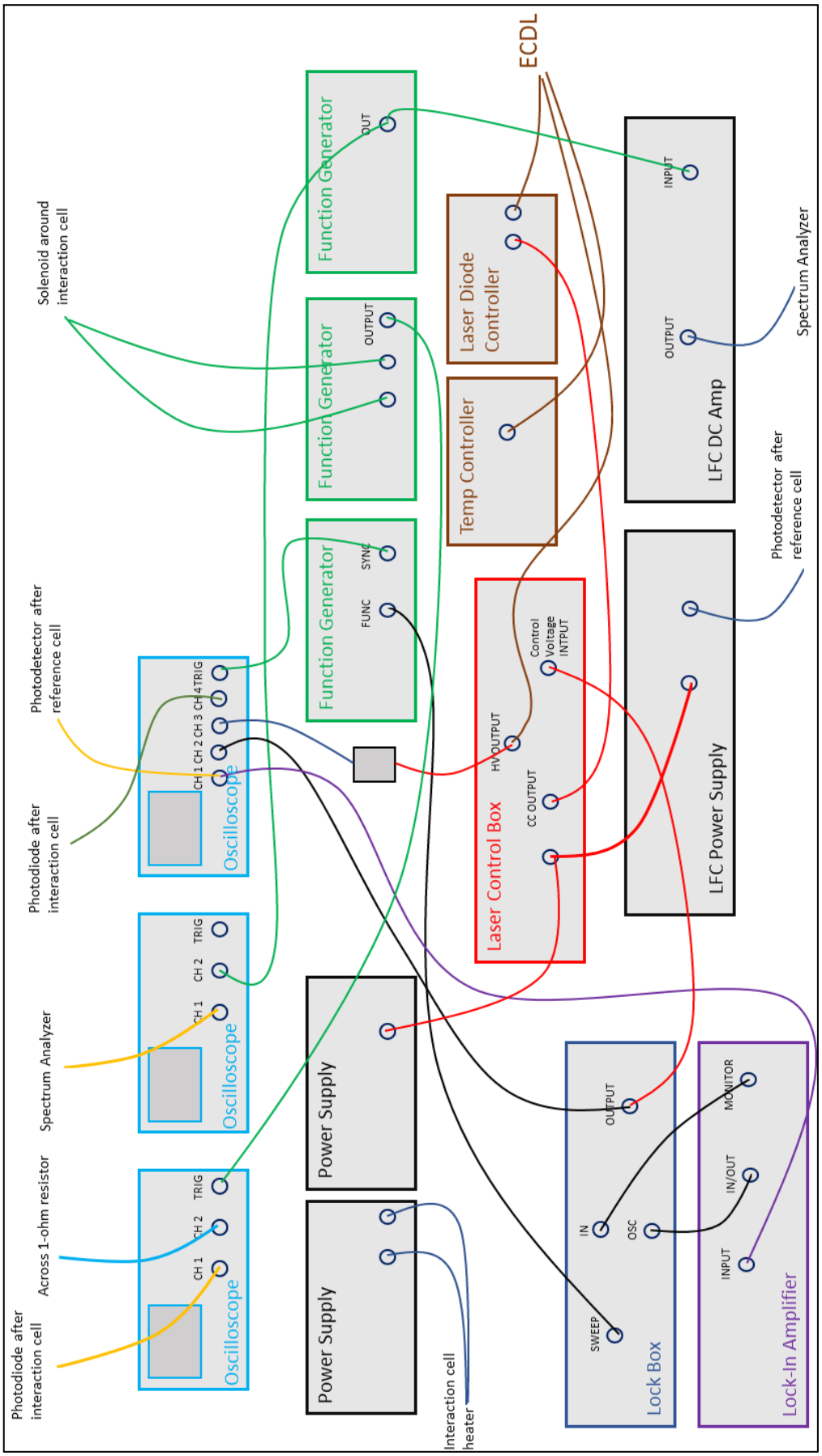

FIG. 17. Diagram of the instrumentation setup.

F. Electronic Instrumentation

Figure 17 above illustrates the connections from each device in the setup to the instrument that controls it. This shows our ability to adjust different pieces of the experiment to achieve EIT and how the instruments in the experiment are connected. The instrumentation setup consists of three power supplies: one LFC home-built and two Agilent DC Power Supplies (Model E3611 and E3612). These are used to power the interaction cell heater, the laser control box, the photodetector after the reference cell, and the spectrum analyzer. Three function generators are also used in the setup: Design Mate 2 Function Generator, Pasco Scientific Model PI-9587B Digital Function Generator, and Stanford Research Systems 30MHz Model DS345 Synthesized Function Generator. The Design Mate 2 sends a function to the LFC DC Amplifier that drives the spectrum analyzer to monitor the laser frequency. The Pasco Scientific is used to sweep the magnetic field of the solenoid around the interaction cell. The Stanford Research Systems is used as the sweep of the lock box. Next we have a ThorLabs Model TEC2000 Temperature Controller and ThorLabs Model LDC500 Laser Diode Controller to control the temperature and current of the ECDL. The Laser Diode Controller is also connected to the Laser Control Box so that the current can be adjusted more precisely. The LFC-built laser control box allows us to finely adjust the gain and bias of the PZT and current controller. Then we have an LFC home-built lock box that serves as the input of the laser control box and provides a smoothly adjustable control voltage to adjust the laser frequency. Lastly, we have three Tektronix Two Channel Digital Oscilloscopes (TDS 2002B, TDS 220, and TDS 2004B) to monitor the transmission through the reference cell, transmission through the interaction cell, voltage across the 1-ohm resistor, and to observe EIT.

IV. EXPERIMENT

A. Polarized light

In this experiment, polarization of light plays a significant role. Achieving high quality linear polarization is a key part of our setup. This can be achieved using linear polarizers, which allow light waves of a particular polarization through and block all other polarizations. Another device used in our experiment is a polarizing cube beam splitter (PCBS). This takes one input beam and separates it into two perpendicular output beams; one horizontally polarized and the other vertically polarized with respect to the laser table. It acts as two linear polarizers, one for each output beam. In order to achieve two output beams that are equal and maximized in intensity, we look at Malus's Law:[8]

$$I = I_o \cos^2 \theta \tag{10}$$

where I_o is the intensity of the incident light, I is the intensity of the transmitted light, and θ is the angle between the transmission axis of the polarizer and the polarization of the incident light. Ideally, if the incident light is polarized $45°$ from the transmission axis, each output will be maximized and have the same intensity. If the incident light were unpolarized, the output would still be two linearly polarized beams, but they may not be equal in power. In our experiment, a PCBS was used to get two equal-intensity linearly polarized and orthogonal beams, one with vertical polarization and one with horizontal polarization with respect to the laser table. We also used linear polarizers in our setup to ensure that each beam was perfectly vertically or horizontally polarized.

In our experiment, circularly polarized light is achieved using a ThorLabs Soleil-Babinet Compensator (SBC). Using the SBC with two orthogonal input beams, we get left and right circularly polarized light. As noted previously, right circularly polarized

light is when the electric field appears to rotate in a clockwise direction when looking into the source and left circularly polarized light is when the electric field appears to rotate counterclockwise when looking into the source.

The following steps are taken to set up the SBC to give us circularly polarized light:

1. Set up crossed polarizers by rotating one polarizer until we obtain maximum power transmitted and then add the analyzer (another polarizer after the first one) and rotate that one until we obtain minimum transmitted power.
2. Insert the SBC between the two polarizers, which results in some transmitted power through the analyzer.
3. Rotate the SBC until the transmission is minimized.
4. Rotate the SBC 45 degrees, adjust the micrometer on the SBC until the power is minimized again, and set that position to zero.
5. Continue rotating the micrometer until we find another minimum in transmission. That distance gives us one full wave of retardance at the wavelength of the laser. The retardance is the phase shift between the two polarized components that are transmitted.
6. Set the position of the micrometer to be a quarter of this distance, which sets up the SBC to give us circularly polarized light.

1. Testing circular polarization

We put much effort into getting the best quality circularly of polarized light possible. To do so, we first started with a HeNe laser, ThorLabs Glan-Thompson polarizer, analyzer (another ThorLabs polarizer downstream), and ThorLabs Model SBC-

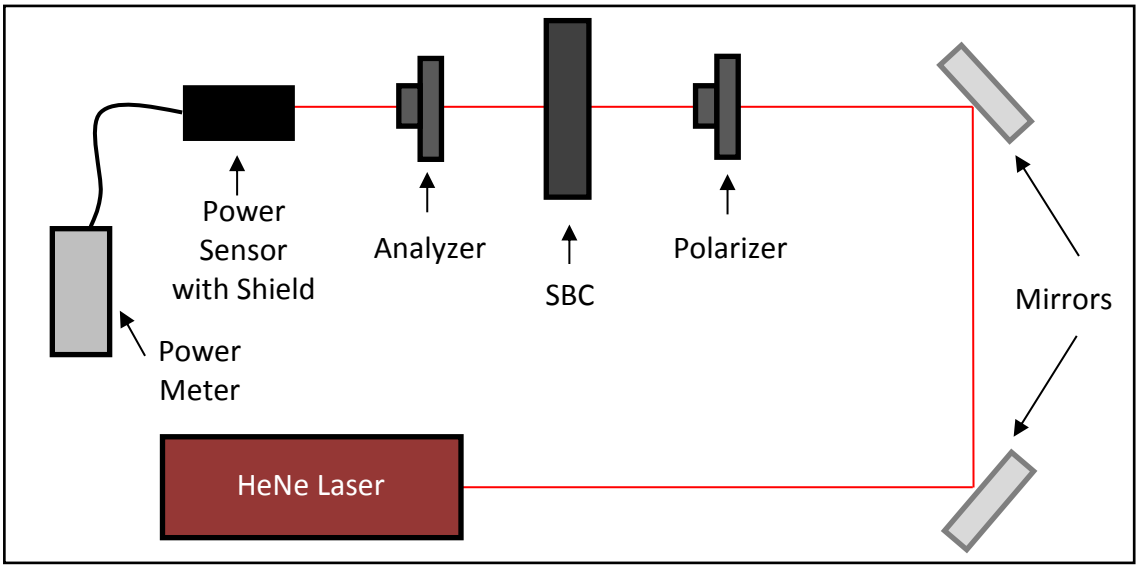

FIG. 18. Test setup for achieving circular polarization. We used a HeNe laser, two mirrors, a polarizer, a Soleil-Babinet Compensator (SBC), an analyzer (a polarizer downstream), and a power sensor with a shield to block room light and a power meter.

VIS Soleil-Babinet Compensator (as shown in FIG. 18) to test the quality of circular polarization that is achievable. Ideally, when circular polarization is attained, the intensity of the transmitted light does not depend on the analyzer angle. Therefore, the ideal result would give us a flat line when we plot transmitted power vs analyzer angle.

Using this setup, we recorded the transmitted power when rotating the analyzer in 10 degree increments. We used a ThorLabs PM100 Power Meter and PM100 software to record the power by measuring it over 12.5 seconds and taking the average. Plotting transmitted power vs analyzer angle gave us a graph without much deviation from the mean (FIG. 19), indicating good quality of circular polarization. We took two trials on two different days and found similar results, indicating there is not a systematic problem with our circular polarization. The fluctuations in transmitted power were about 4% peak to peak from the mean.

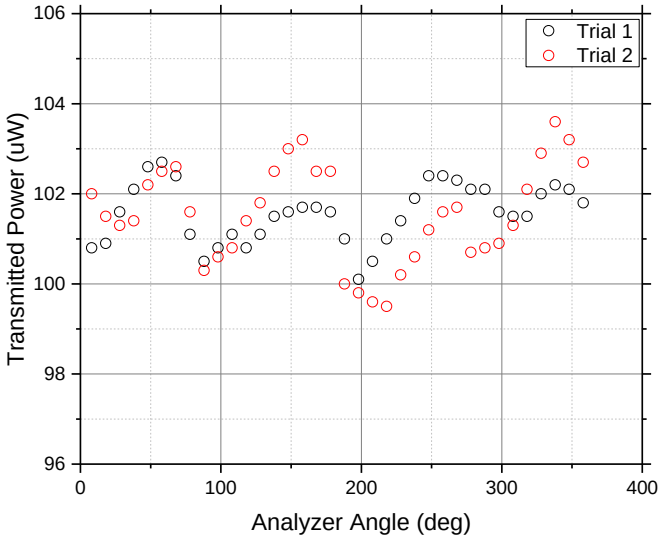

FIG. 19. Measurement of circular polarization using a HeNe laser.

This quality, however, seems to decrease when we try to achieve the other (left or right) circular polarization by rotating the SBC 90°. The graph of transmitted power vs analyzer angle (FIG. 20) is not as flat for this setup and has a more distinct sine wave pattern. In this case the fluctuations in transmitted power were about 16% peak to peak from the average transmitted power.

To test the accuracy of the SBC we repeated the measurements when rotating the

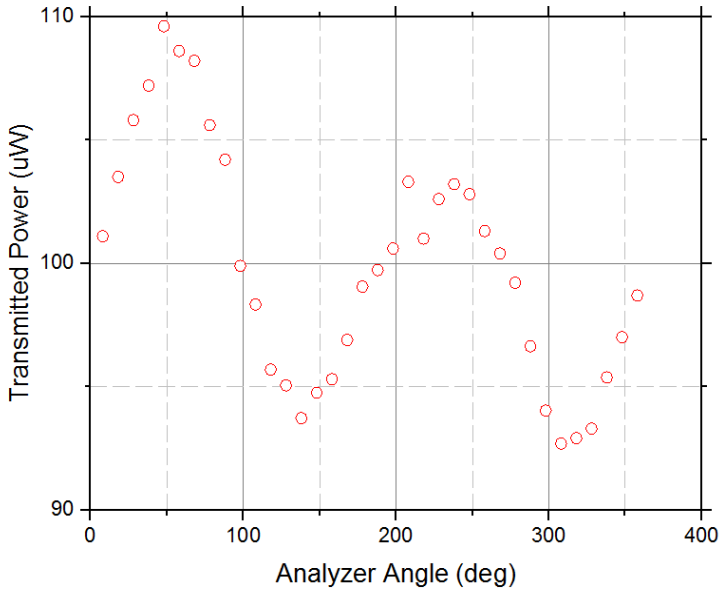

FIG. 20. Measurement of circular polarization using a HeNe laser.

SBC $89°, 89.5°, 90.5°,$ and $91°$. These each gave fluctuations greater than the 16% peak to peak that was attained when originally rotating it $90°$. Therefore, we concluded that simply rotating $\pm 90°$ gives the best results for left and right circular polarization.

2. Analyzing input linear polarization

Next, we used this procedure for the external cavity diode laser (ECDL), which we used in our apparatus for this experiment. Before achieving our circular polarization with this setup, however, we first tested the quality of linear polarization going into the SBC. To do so we removed the SBC from the setup and recorded the transmitted power as a function of analyzer angle. As before, we rotated the analyzer $10°$ between each measurement and took the average of the transmitted power over 12.5 seconds. Our first measurements gave results indicating a problem with our linear polarization, as shown in FIG. 21. When rotating the analyzer, the transmitted power should follow a $\sin^2\theta$ pattern. When we plotted the ratio of transmitted to maximum transmitted power versus analyzer angle, however, our graph shows that the transmitted power through the analyzer does not reach the same peak when rotating the analyzer $180°$. This indicated a problem we needed to solve in our setup of linear polarization. We also recorded data for a few of the analyzer angles at the beginning and at the end to check for drift. As can be seen in the data points for a few of the first analyzer angles, the points overlap quite well. It is not possible to see the difference in some cases. From this, we concluded that the problem with our linear polarization was not due to any instability in our laser; rather our laser seemed to be quite steady.

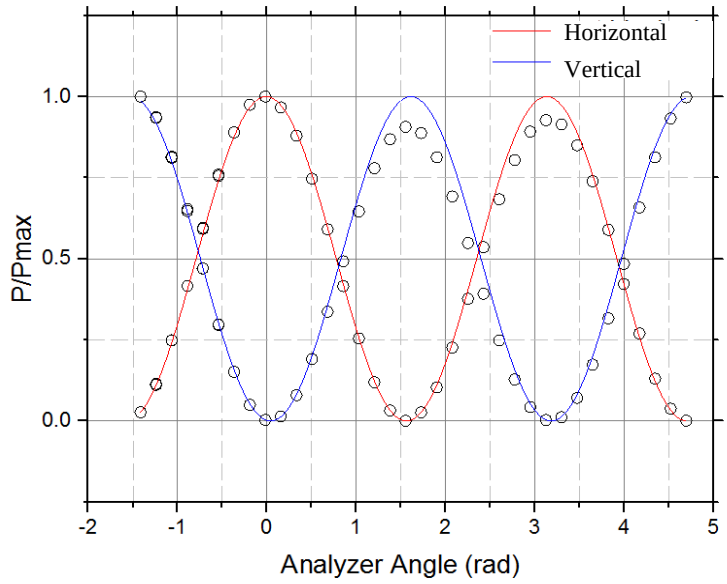

FIG. 21. Graph of power vs analyzer angle when testing the quality of linear polarization of the horizontally and vertically polarized input beams of the ECDL laser.

In order to correct this problem, we went through a series of adjustments. The first change was to check that the beam passed through the polarizer correctly. The method to do this was to put a piece of paper between the mirror and the analyzer that had a hole in it so that the beam could still get through. We could then see the reflected beam from the analyzer on the paper. Aligning the reflected beam with the input beam for all angles of the analyzer was not achievable using this method. After upgrading to a kinetic mount for the analyzer, and aligning the reflected beam from it, we were able to fix the problem. Repeating the same measurements as before, the data now reach the same maximum and follow the $\sin^2\theta$ curve very well (FIG. 22).

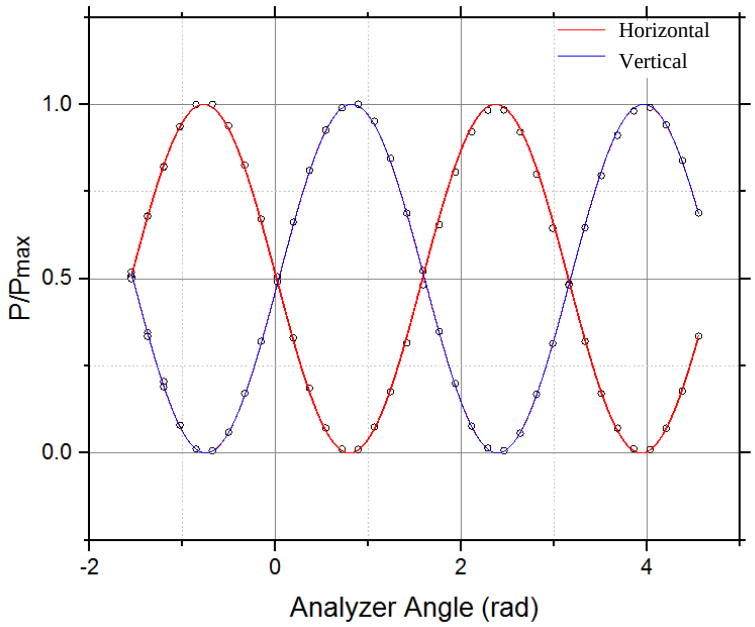

FIG. 22. Plot of power vs analyzer angle when testing the quality of linear polarization of the horizontally and vertically polarized input beams of the ECDL laser.

3. Analyzing input circular polarization

Once we were confident with the good quality of linear polarization we were making, we moved onto achieving the best quality of circular polarization from the ECDL laser as possible. In this setup, we had a horizontally polarized beam and a vertically polarized beam going into the SBC and analyzer. Therefore, to set up the SBC we needed to block one of the beams, in this case we blocked the vertically polarized beam. Then, after setting up the SBC, we tested the right and left circular polarization one at a time by blocking the vertically polarized beam, recording data, and then repeating with the horizontally polarized beam blocked. The graph of transmitted power vs analyzer angle (FIG. 23) shows results with some improvement to the graph for the HeNe laser. When we had the horizontal beam (producing right circular polarization from the SBC), our fluctuations in transmitted power were 8% peak to peak from the average. When we had the vertical beam (producing left circular polarization), our fluctuations

were 13% peak to peak from the average transmitted power. Therefore, we decreased the fluctuations in the right circularly polarized light by half from the practice trial with the HeNe laser.

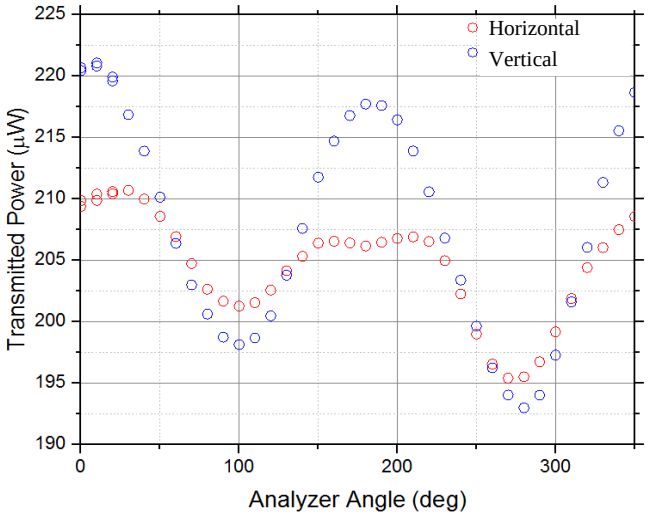

FIG. 23. ECDL laser used to achieve left and right circularly polarized light by blocking the horizontally polarized and vertically polarized input beams, one at a time.

4. Analyzing output linear polarization

Once we had this good quality of circular polarization, we sent the circularly polarized light through the interaction cell. After it went through the cell, it needed to be linearly polarized again. This was achieved using a ThorLabs Model SAQWP05M-1700 quarter-wave plate placed directly after the cell. In order to evaluate the quality of the linear polarization we got, we repeated the same procedure as above using an analyzer and power meter, to get the transmitted power vs analyzer angle. We plotted this data and see (in FIG. 24) that it fits well with the $\sin^2\theta$ curve. The quality is slightly poorer than the linear polarization we analyzed going into the SBC. One explanation for this is that the quarter-wave plate we used is a 780 nm quarter-wave plate, whereas our laser beam has a wavelength of 795 nm. This difference could be the cause of why we did not get as high a quality. In any case, this linear polarization is certainly sufficient for the purposes

of this experiment.

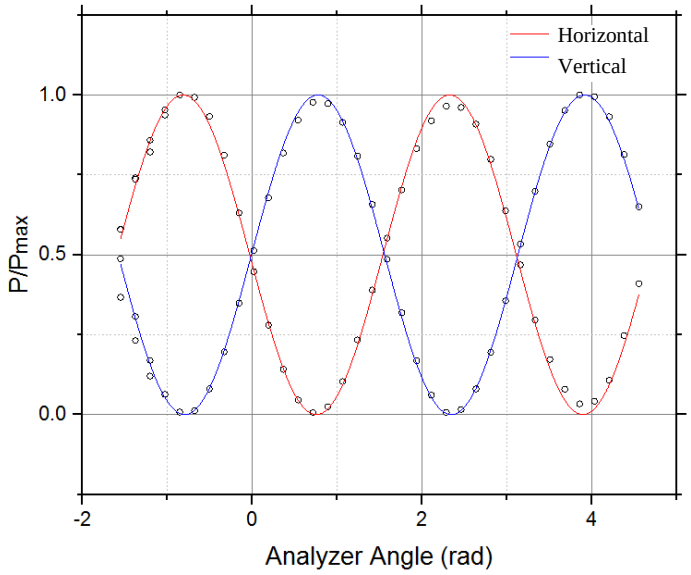

FIG. 24. Testing the quality of linear polarization of the horizontally and vertically polarized beams reconstructed after the interaction cell.

B. EIT

To achieve electromagnetically-induced transparency (EIT), we used a Pasco function generator to sweep the magnetic field inside the interaction cell. The magnetic field induces the Zeeman Effect, causing the splitting in the hyperfine structure of the ^{87}Rb atoms needed to observe EIT. Using a Tektronix oscilloscope, we monitored the transmission through the interaction cell and the voltage across a 1-ohm resistor in series with the solenoid. The 1-ohm resistor gives us the ability to calculate the magnetic field inside the solenoid. Figure 25 shows a scan of the first time we achieved EIT. The main goal of this experiment was to characterize the parameters that led to achieving optimum EIT. The next sections will do that. As we know, the spike in the observed spectrum corresponds to high transmission through the cell. By optimizing EIT, we were trying to get as much transmission as possible.

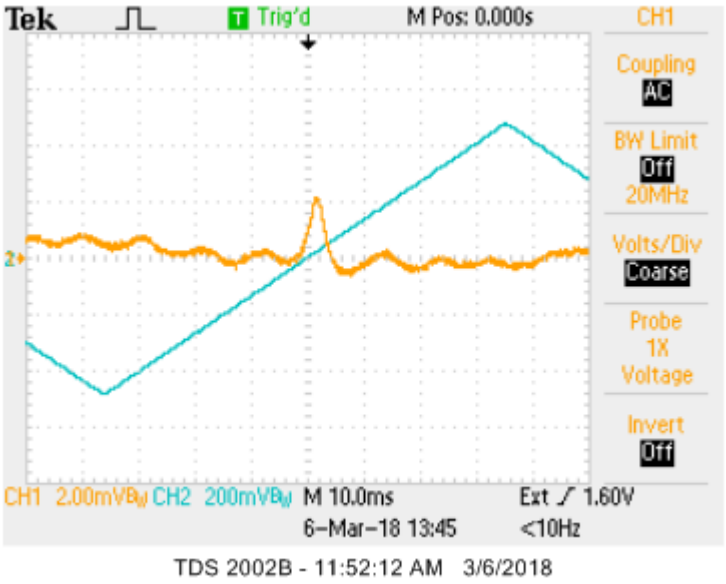

FIG. 25. A scan of the first time EIT was achieved. Channel 1 monitors the transmission through the interaction cell. Channel 2 monitors the voltage across the 1-ohm resistor.

1. *Room lights and EIT*

After achieving EIT, the first condition we tested was whether having the room lights on in the lab affected the transmission observed from the photodiode. Figure 26 shows a scan when the lights were on and when the lights were off. Comparing these scans, it was clear that room lights did not affect the reading from the oscilloscope when it is AC coupled. Therefore, the rest of our testing was done with the room lights on.

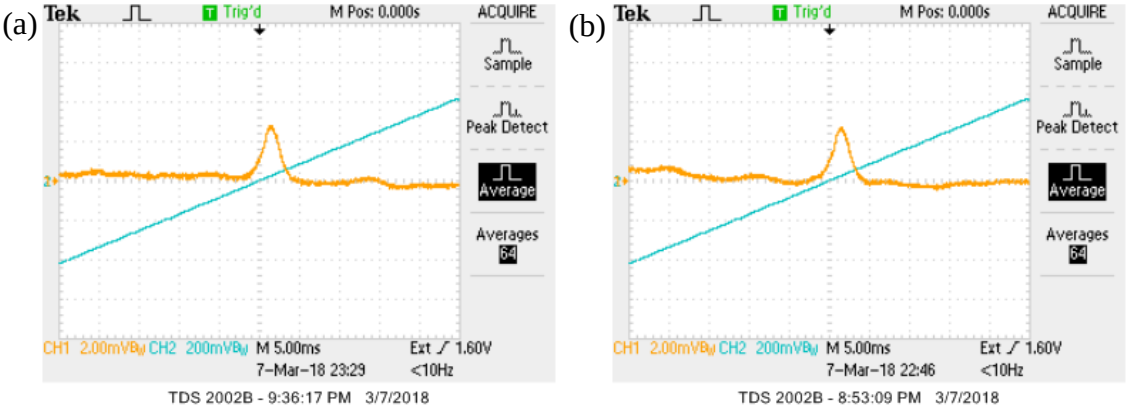

FIG. 26. Scan of EIT when (a) room lights are on and (b) room lights are off.

2. *Temperature of the rubidium interaction cell*

Inside the solenoid of the interaction cell, there is a thermistor that is used to control the heating of the cell of rubidium atoms. A thermistor is a type of resistor whose resistance depends on, and is inversely related to, its temperature. Therefore, to determine the temperature of the thermistor we first measured the voltage across and the current through the thermistor. Using Ohm's Law, $V = IR$, we calculated the resistance of the thermistor. Next, we used the formula for a thermistor,

$$R = R_o e^{B\left(\frac{1}{T}-\frac{1}{T_o}\right)}, \tag{11}$$

where R is the resistance of the thermistor at any temperature, T, and the constants B, T_o,

and R_o are specified for the type and model of thermistor. For our thermistor, these values are $B = 3974$, $T_o = 298.15\,\text{K}$, and $R_o = 10.00\,\text{k}\Omega$. Rearranging this equation for temperature, T, we obtained the following equation:

$$T = \frac{1}{\frac{1}{T_o} + \frac{1}{B}\ln(\frac{R}{R_o})} \tag{12}$$

This allowed us to calculate the temperature of the thermistor at any resistance, R. Therefore, by monitoring the voltage and current through the thermistor, we could easily calculate the temperature of the thermistor and the interaction cell. For example, at one point we measured the voltage and current to be 0.862 V and 0.28 mA, respectively. Using Ohm's Law, the resistance was therefore calculated to be 3079 Ω. Lastly, equation (4) gave us the temperature of the thermistor to be 327 K or 54˚C.

3. Density of atoms

Next, we wanted to calculate the density of the ^{87}Rb atoms inside the interaction cell. To do so, we first used the following equation to calculate the vapor pressure in Pascals:[9]

$$\log_{10}(P_v / \text{Pa}) = a + b - \frac{c}{T}, \tag{13}$$

where P_v is the vapor pressure in Pascals, T is the temperature in Kelvin and a, b, and c are constants. For ^{87}Rb above its melting point of 39.3˚C, $a = 5.006$, $b = 4.312$, and $c = 4040$ K. We then calculated the number density using,

$$\rho_N = \frac{N}{V}\ , \tag{14}$$

where ρ_N is the number density, N is the total number of atoms, and V is the volume. Combining this equation with the Ideal Gas Law,

$$PV = NkT\,, \tag{15}$$

we get our final equation,

$$\rho_N = \frac{P_v}{kT}\,, \tag{16}$$

where ρ_N is the number density in m^{-3} and k is Boltzmann's constant. Using this equation, and converting to cm^{-3}, we calculated the number density inside the cell to be $2.04\times10^{11}\ \mathrm{cm}^{-3}$ at 54 ˚C.

4. Temperature and EIT

Once we knew how to calculate the temperature inside the interaction cell, we could use this to analyze what effect the temperature had on the quality of EIT. The temperature of the cell started at about 53 ˚C and was increased to 70 ˚C. Figure 27 shows a scan recorded at each temperature, clearly depicting an increase in transmission through the cell. Since we knew the horizontal beam was transmitted through the PCBS, we were monitoring the horizontal beam in these scans. The peak transmission in the first scan was 2.80 mV and the peak transmission in the second scan was about 7.36 mV. As the temperature increased, the density of atoms in the interaction cell increased from $1.87\times10^{11}\ \mathrm{cm}^{-3}$ to $7.18\times10^{11}\ \mathrm{cm}^{-3}$. The increase in transmission also showed more asymmetry occurring before and after the peak.

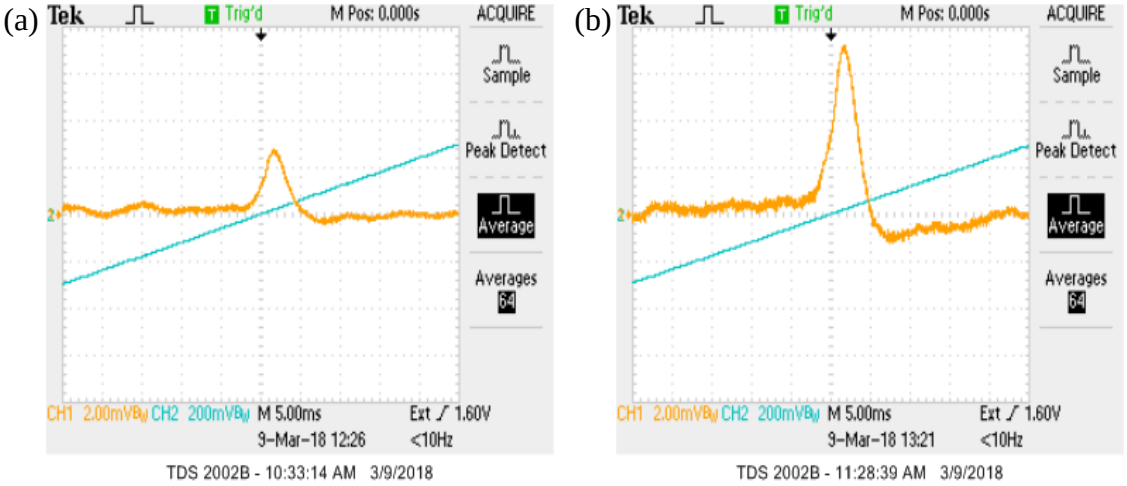

FIG. 27. Scan of the transmission through the interaction cell when the thermistor is at (a) 53˚C and (b) 70˚C.

Repeating this experiment on a different day, we again increased the temperature and observed the effect it had on our transmission through the interaction cell. This time the temperature of the thermistor started at about 69 ˚C and was increased to 75 ˚C. The scans before and after are shown in FIG. 28 and the peak intensity increased from 6.32 mV to 7.92 mV**.** In this case, the density inside the cell increased from about 6.89×10^{11} cm^{-3} to1.09×10^{12} cm^{-3}.

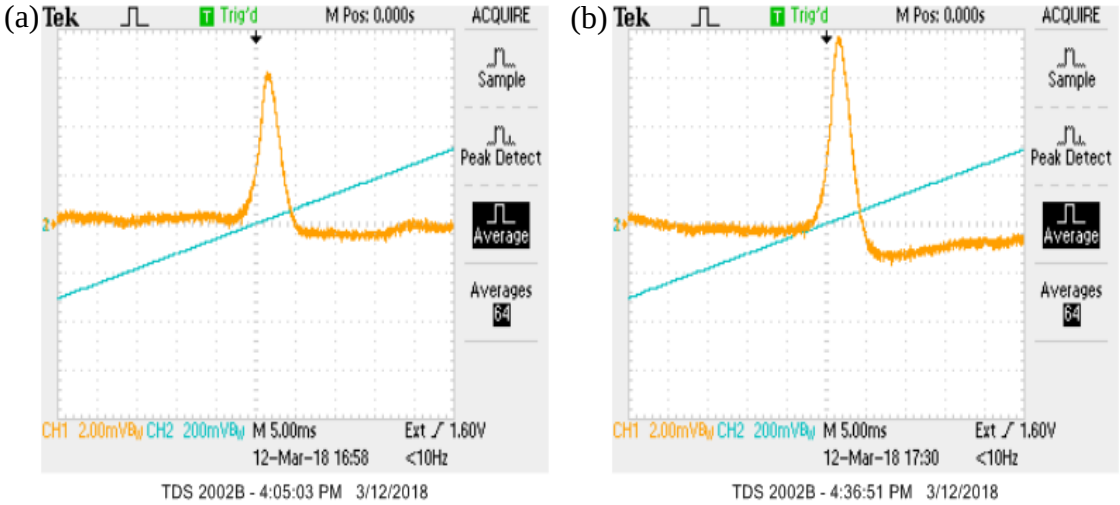

FIG. 28. Scan of the transmission through the interaction cell when the thermistor is at (a) 69 ˚C and (b) 75˚C.

On a third day, we repeated this experiment a third time, again observing the effect of increasing the temperature inside the interaction cell. The temperature started at 79 ˚C and was increased to 83 ˚C. Since this is a small change in temperature, the difference in the scans in FIG. 29 is not very noticeable. The recorded peak transmission, however, increased from 7.92 mV to 8.26 mV. Note that the vertical scale in these scans has been changed from the previous ones, namely one box now represents 5.00 mV instead of 2.00 mV. In this case, the density inside the cell increased from 1.44×10^{12} cm^{-3} to 1.88×10^{12} cm^{-3}.

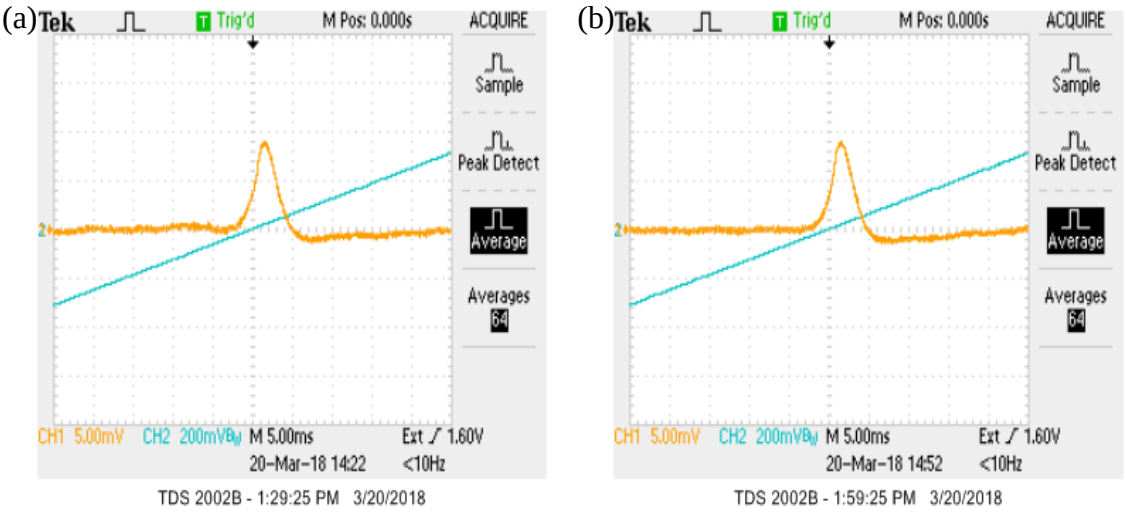

FIG. 29. Scan of the transmission through the interaction cell when the thermistor was at (a) 79 ˚C and (b) 83˚C.

After completing these experiments we calculated the change in transmission (ΔV) per change in temperature (ΔT) for each of the three trials. For the first trial (53˚C to 70˚C) we calculated a value of 2.72×10^{-4} V/˚C, for the second trial (69 ˚C to 75 ˚C) we calculated 2.61×10^{-4} V/˚C, and for the last trial (79 ˚C to 83 ˚C) we calculated 5.96×10^{-5} V/˚C. As the temperature increased, these values decreased. This indicated that increasing temperature had a bigger effect (per degree Celsius) on transmission through the cell until a certain point. After this point, the change did not increase the transmission as much, per unit temperature.

5. Neutral density filter and EIT

The next condition we tested was to see what effect using a neutral density filter to change the amount of power from each input beam (vertically and horizontally polarized) had on the EIT signal. A neutral density filter is simply a filter that decreases the intensity of light of all wavelengths that get through it by the same amount. Neutral density filters are labeled by their optical density (OD), which defines the amount of power blocked by the filter. From the optical density, we can calculate the percent transmission, T, that gets through the filter by the following equation:[10]

$$T = 10^{-OD} \cdot 100\% . \tag{17}$$

First, we took a scan to record the EIT signal without any filter. Next, we placed a neutral density filter in the horizontal beam between the PCBS and mirror in the signal and control field generation section of the apparatus. We measured the power of the beam going into the interaction cell without any filters, and then the power of the beam going into the interaction cell when each neutral density filter was changing the power of the horizontally polarized beam. We used a PM100 Power Meter and recorded the average power over 7.5 seconds. For each filter, we then let the beam through the interaction cell and monitored the effect. FIG. 30 shows the scans of transmission through the interaction cell for each neutral density filter.

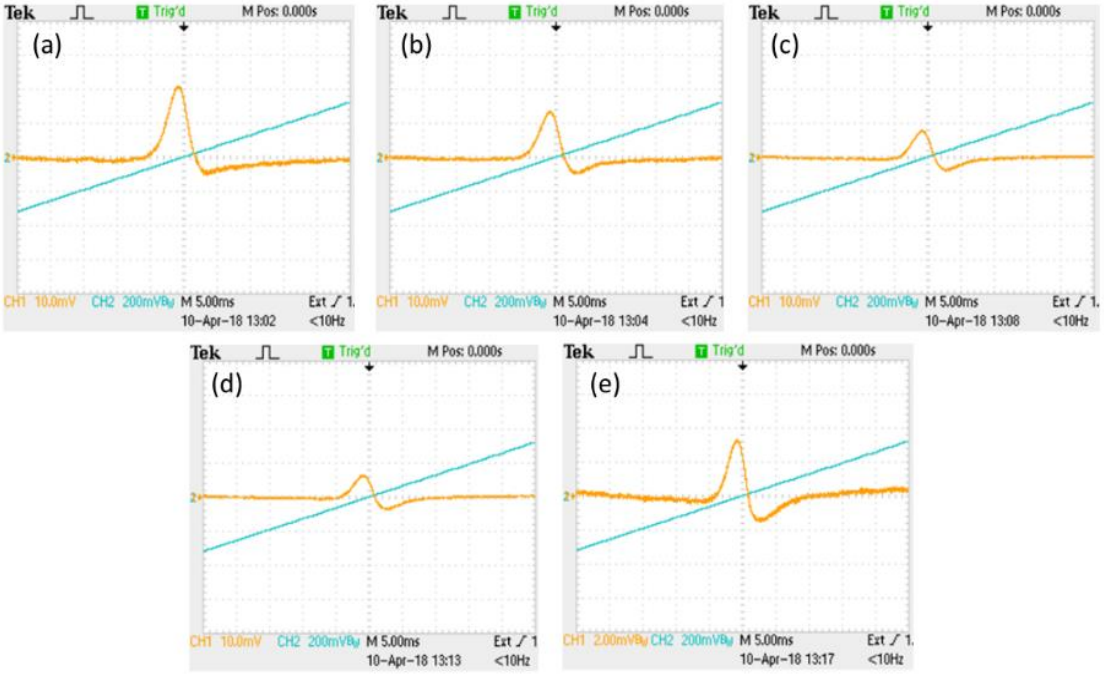

FIG. 30. Scan of the transmission through the interaction cell when a neutral density filter in the horizontal beam with an optical density of (a) 0, (b) 0.2, (c) 0.5, (d) 0.6, and (e) 1.0 was changing the power of the horizontally polarized beam. Carefully note the vertical scale of channel 1 in (e).

As expected, the transmission through the cell decreased when the power of the horizontally polarized beam was decreased. The scans also seem to show that filtering the horizontal beam did not have any effect on the asymmetry in the transmission. Data on the power of the beam going into the cell for each filter, as well as the peak of the EIT signal, is shown in Table I.

Filtering Horizontal Beam			
Optical Density of Filter, OD	Percent transmission of filter, T (%)	Power of beam into cell (mW)	Peak of EIT signal (mV)
0	100	4.53	20.8
0.2	63.1	3.82	13.6
0.5	31.6	3.30	8.00
0.6	25.1	3.15	6.80
1.0	10	2.83	3.36

Table I. Results of the power of the beam going into the interaction cell as well as the peak of the EIT signal when each filter changed the power of the horizontally polarized beam.

We repeated the same process, but placed the neutral density filters in the vertical beam instead. The scans of transmission through the interaction cell for each filter are shown in FIG. 31.

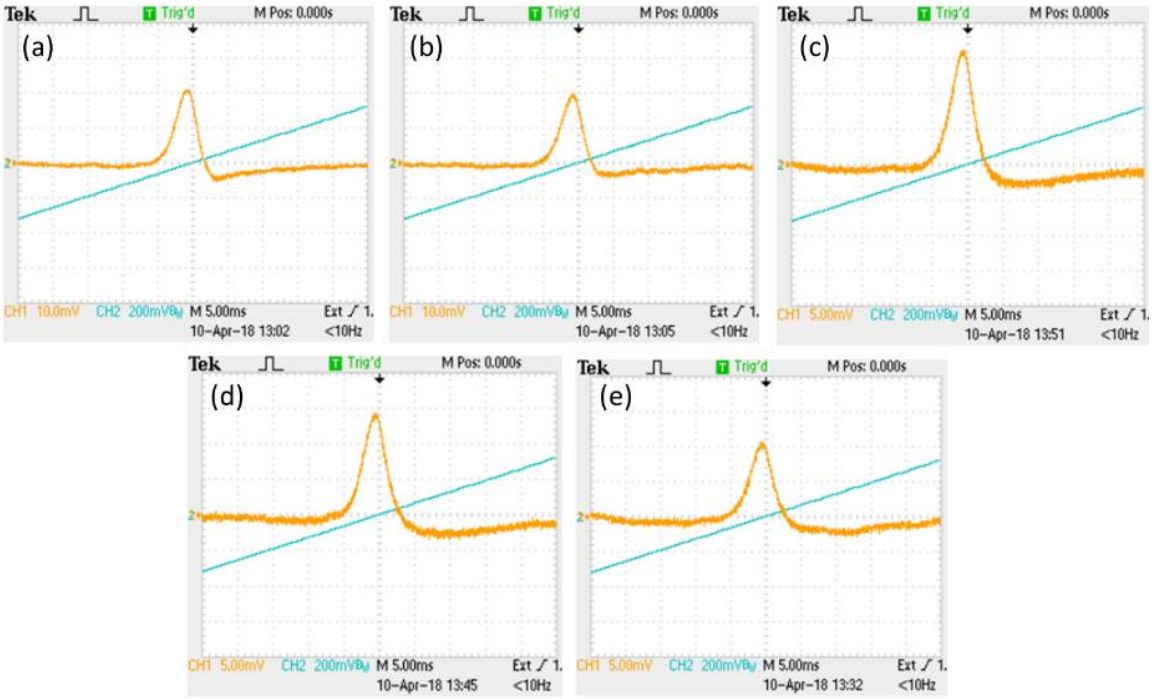

FIG.31. Scan of the transmission through the interaction cell when a neutral density filter in the vertical beam with an optical density of (a) 0, (b) 0.2, (c) 0.5, (d) 0.6, and (e) 1.0 was changing the power of the vertically polarized beam. Note the vertical scale is not the same across each scan.

As when we changed the horizontally polarized beam, the transmission through the cell decreased when the power of the vertically polarized beam was decreased. As shown in Table II, however, the peak of the EIT signal did not decrease as much. When the 1.0 optical density filter changed the vertical beam, the peak EIT signal was approximately 50% of the peak signal without a filter. When the same filter changed the horizontal beam it gave a peak EIT signal around 15% of the unchanged signal. Data on the power of the beam going into the cell for each filter, as well as the peak of the EIT signal, is shown in Table II.

Filtering Vertical Beam			
Optical Density of Filter, OD	Percent transmission of filter, T (%)	Power of beam into cell (mW)	Peak of EIT signal (mV)
0	100	4.53	20.8
0.2	63.1	3.67	19.2
0.5	31.6	3.02	16.8
0.6	25.1	2.83	14.4
1.0	10	2.44	10.8

Table II. Results of the power of the beam going into the interaction cell as well as the peak of the EIT signal when each filter changed the power of the vertically polarized beam.

The scans also seem to show that filtering the vertical beam decreased the asymmetry in the transmission. To explore this more analytically, we measured the minimum (most negative) point of the signal. Ideally, this would be zero if our transmission was symmetric about the y-axis. Therefore, we aimed to estimate the asymmetry by the ratio of the size of the "dip" that is visible on the right side to the peak of the signal. These results are shown in Table III. The results show that the ratio is, in fact, significantly smaller when the vertically polarized beam was filtered.

Optical Density of Filter, OD	0	0.2	0.5	0.6	1
Percent transmission of filter, T (%)	100	63.1	31.6	25.1	10
	Filtering Horizontal Beam				
Ratio of dip to peak	0.25	0.38	0.55	0.47	0.48
	Filtering Vertical Beam				
Ratio of dip to peak	0.25	0.21	0.19	0.22	0.24

Table III. Results of the ratio of the dip to the peak of the EIT signal when both the horizontally polarized and vertically polarized beam were changed.

6. Size of the beam

Another parameter we wanted to investigate in this experiment is the size of the laser beam we were using. In order to do so, we used a Caliens Linear CCD Camera. The CCD camera allowed us to measure the beam over its 30 mm range. We placed the CCD camera before the interaction cell to measure the size of the beam entering the cell. Initially the power of the beam was too high for the camera, so we placed three neutral density filters before the SBC (and camera) to reduce the power of the beam. A plot of the data acquired from that beam is shown in FIG. 32. In many cases, ideal laser beams have a Gaussian intensity distribution. Therefore, we fit our plot to a Gaussian function and from that we obtained our measured beam radius.

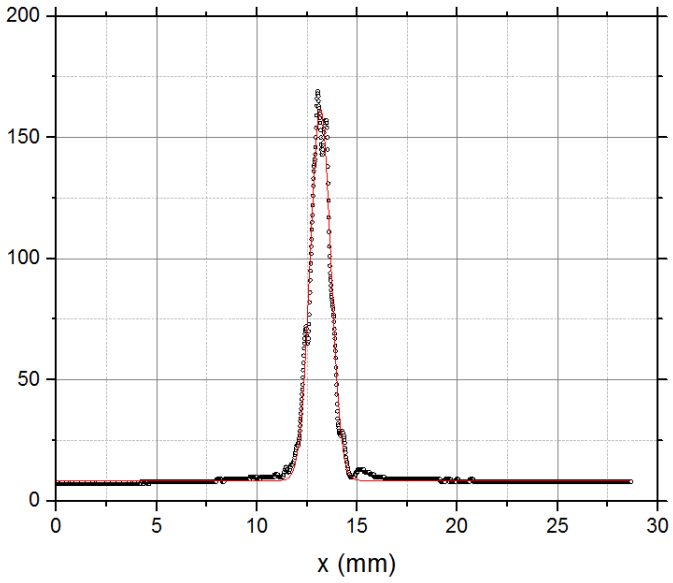

FIG. 32. Measurement of power of the laser beam as a function of the position in the laser beam from the CCD camera.

To investigate whether we were getting consistent reading of the size of the beam, we placed the CCD camera on a translational stage and measured the beam multiple times, moving it 5 mm in between each measurement. Based on this test, we found that the results were consistent among the 5 trials. Plotting all 5 trials on the same graph shows that the shape of the profile of the beam did not change when simply moving the

camera (FIG. 33). As expected, it simply shifted where the peak is located on the detector. We calculated the diameter of the beam for each of these 5 trials and found the average to be 2.07 mm.

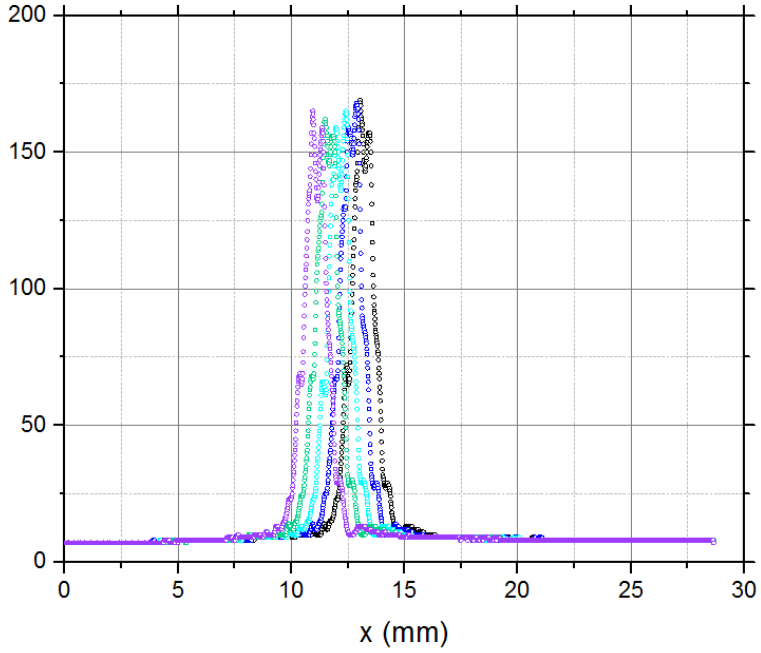

FIG. 33. Measurements from the CCD camera of power of the laser beam as a function of the position in the laser beam for five different locations of the camera (we moved the camera 5 mm between each trial).

Next, we rotated the CCD camera 90 degrees to measure the perpendicular diameter of the beam. This allowed us to determine whether our beam had a circular or elliptical cross section. As discussed in The Apparatus section, we use an anamorphic prism pair to reshape the beam from elliptical to circular. These measurements told us how circular the beam actually becomes. We took 3 trials measuring the diameter and found that the average value was 2.24 mm. This suggested that the beam is not perfectly circular, and rather still has a slightly elliptical shape.

Using the data we collected for the width of the beam measured perpendicular to each other, we calculated the cross sectional area of the beam. The area of an ellipse is

$$A = \pi ab \tag{18}$$

where a is the length of the semi-major axis and b is the length of the semi-minor axis. We calculated the cross-sectional area to be $3.64\,\mathrm{mm}^2$.

We then wanted to investigate the size of the beam after it passed through the interaction cell. This time the CCD camera was placed directly after the PCBS. The same process for measuring the beam before the cell was repeated. The average of the 5 measurements (again moving the camera 5mm between each) gave us a width of 3.04 mm. After rotating the camera 90 degrees, we measured a width of 3.25 mm. Therefore, these measurements agree with the measurements before the cell that the beam has an elliptical shape with its semi-major axis parallel to the laser table. The calculated cross sectional area of the beam after the cell was $7.75\,\mathrm{mm}^2$. The size of the beam increases as it goes through the interaction cell, which simply tells us that the beam does not have a focus inside the cell.

7. Sweeping frequency

Another interesting parameter to note is the effect of the sweeping frequency on the EIT signal. The sweeping frequency defines the frequency at which we sweep the magnetic field in the solenoid inside the interaction cell. For all the measurements in this experiment, the frequency was set to 7.0 Hz. In this section we tested how changing that frequency would affect our signal. To do so, we took a scan of the signal at 7.0 Hz, then decreased the frequency to 0.7 Hz, and lastly increased the frequency to 70 Hz. The scans of each are shown in FIG. 34.

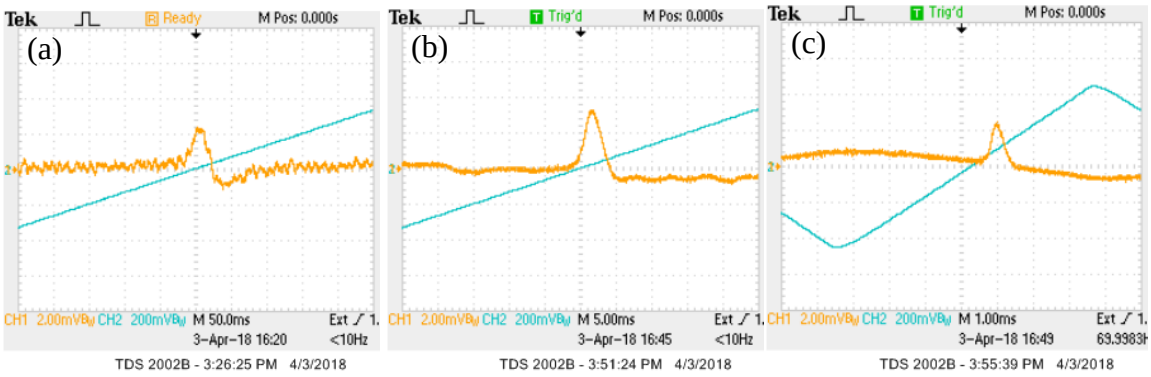

FIG. 34. Scans of the EIT signal at a frequency sweeping the magnetic field in the interaction cell of (a) 0.7 Hz, (b) 7.0 Hz, and (c) 70 Hz.

V. CONCLUSION

We successfully characterized some parameters that affect the amount of transmission we get through our interaction cell of rubidium, when the conditions for EIT are met. This gives us measurements that can lead to our goal of being able to predict how much transmission is expected in future study. Future investigation could include similar calculations and parametrization for EIT achieved with an interaction cell of purely isotopic ^{87}Rb and 5-torr He buffer gas. Slow light should also be achievable with the current setup.

VI. REFERENCES

[1] D. J. Griffiths, *Introduction to Electrodynamics*, 4th ed. (Pearson Addison Wesley, Upper Saddle River, NJ, 2013), Equation 8.10, p. 358

[2] D. S. Kliger, J. W. Lewis, C. E. Randall, *Polarized Light in Optics and Spectroscopy*, (Academic Press, Inc., San Diego, CA, 1990), p. 13-14.

[3] M. D. Lukin, *Colloquium: Trapping and manipulating photon states in atomic ensembles*, Reviews of Modern Physics, Volume 75, April 2003.

[4] D. A. Steck, *Rubidium 87 D Line Data*, available online at http://steck.us/alkalidata (revision 2.1.5, 13 January 2015). p. 25-26.

[5] D. J. Griffiths, *Introduction to Quantum Mechanics*, 2nd ed. (Pearson Prentice Hall, Upper Saddle River, NJ, 2005).

[6] K. Spotts, Thesis Lake Forest College (2014), p. 17.

[7] Artifex Engineering (2016).

[8] E. Hecht, *Optics*, 2nd ed. (Addison-Wesley, Reading, MA, 1987), Equation 8.24, p. 278

[9] Alcock, C. B., Itkin V.P., and Horrigan, M. K., *Vapor Pressure Equations for the Metallic Elements: 298-2500 K*, Canadian Metallurgical Quarterly **23**, 309 (1984).

[10] Edmund Optics Worldwide (2018).